Protein storage vacuoles originate by remodelling of pre-existing vacuoles in *Arabidopsis thaliana*

Mistianne Feeney[1,*], Maike Kittelmann[2,*], Rima Menassa[3], Chris Hawes[2], Lorenzo Frigerio[1,€]

[1] School of Life Sciences, University of Warwick, Coventry, CV4 7AL, United Kingdom
[2] Plant Cell Biology, Biological and Medical Sciences, Oxford Brookes University, Oxford, OX3 0BP, United Kingdom
[3] London Research and Development Centre, Agriculture and Agri-Food Canada, London, Ontario, N5V 4T3, Canada
* These authors contributed equally to this work.
[€] Corresponding author: l.frigerio@warwick.ac.uk

Short title: PSV arise from vacuole remodelling

Author contributions

M.F. generated the materials, performed all confocal microscopy and immunogold labelling, contributed to preparation and imaging of EM samples; M.K. prepared and imaged EM and SBF-SEM samples and prepared all reconstructions; R.M. contributed towards generation of the materials; C.H. analysed the data; L.F. conceived the project and analysed the data. All authors contributed to the writing of the manuscript.

One-sentence summary

Protein storage vacuoles originate from a reprogramming of the pre-existing vacuole.

ABSTRACT

Protein storage vacuoles (PSV) are the main repository of protein in dicotyledonous seeds. Little is known about the origins of these transient organelles. PSV are hypothesised to either arise *de novo* or to originate from the pre-existing embryonic vacuole (EV) during seed maturation. We have tested these hypotheses by studying PSV formation in Arabidopsis embryos at different stages of seed maturation and have recapitulated this process in Arabidopsis leaves reprogrammed to an embryogenic fate by inducing expression of the *LEAFY COTYLEDON2* transcription factor. Confocal and immunoelectron microscopy indicate that both storage proteins and tonoplast proteins typical of PSV are delivered to the pre-existing EV in embryos or to the lytic vacuole in reprogrammed leaf cells. In addition, sectioning through embryos at several developmental stages using serial block face scanning electron microscopy reveals the 3D architecture of forming PSV. Our results indicate that in Arabidopsis the pre-existing vacuole is reprogrammed to become a PSV.

INTRODUCTION

During seed development, protein reserves and minerals are stored in specialised vacuoles called protein storage vacuoles (PSV). PSV are functionally different from lytic vacuoles (LV), which are present in most vegetative plant tissues and function as lysosome-like, degradative organelles (Marty, 1999; De, 2000).

PSV exist in both monocots and dicots but are the main site of storage protein accumulation in dicotyledonous species. In spite of the global importance of PSV as primary repositories for storage proteins, very little is known about their origins. It is debated whether they arise *de novo* during seed maturation or whether they derive from the vacuoles present in embryo cells, henceforth named embryonic vacuoles (EV), which undergo a functional reprogramming during seed maturation. Whatever the intracellular origin of PSV, a specific PSV developmental programme must exist, as the simple over-expression of seed storage proteins in non-seed organs is not sufficient to either induce PSV formation or to change the function of the existing LV (Bagga et al., 1992; Frigerio et al., 1998; Frigerio et al., 2000). PSV have been shown to arise by a *de novo* mechanism in cotyledons of developing pea and a similar mechanism may operate in *Medicago truncatula* embryos (Hoh et al., 1995; Frigerio et al., 2008). However, there have been few studies addressing the early stages of PSV formation in Arabidopsis (Mansfield and Briarty, 1992).

In Arabidopsis cells, an EV is present during early embryogenesis (Rojo et al., 2001; D'Ippólito et al., 2017). During the maturation phase of seed development, PSV arise to accumulate storage reserves and ultimately become the only detectable vacuole (Mansfield and Briarty, 1992; Otegui et al., 2006). PSV persist in embryonic cells until seed germination, when reserves are mobilised to provide nutrients for the growing seedling. The PSV-to-LV transition during germination has been studied in tobacco root tip cells: LV were shown to arise by a reprogramming and fusion of PSV (Zheng and Staehelin, 2011). PSV tonoplast markers are also replaced by LV markers in both tobacco and Arabidopsis seedling cells (Gattolin et al., 2011; Zheng and Staehelin, 2011). It is not yet clear whether similar reprogramming mechanisms apply to PSV formation during seed maturation in Arabidopsis.

The study of PSV formation is challenging, as PSV are transient organelles and the EV-to-PSV transition occurs relatively quickly (Mansfield and Briarty, 1992). Genetic approaches have so far not pinpointed the actual formation of PSV. Mutants of ESCRT component FREE1/FYVE1 (Gao et al., 2015; Kolb et al., 2015), SNARE proteins VTI11 and VTI12 (Sanmartin et al., 2007; Zheng et al., 2014) the VAMP727 SNARE complex (Ebine et al., 2008), the δ subunit of the AP-3 adaptor complex (Zwiewka et al., 2011) and the shoot meristem identity protein TFL1 (Sohn et al., 2007), for example, all show a disruption in protein trafficking to PSV, rather than PSV formation. In addition, vacuoleless mutants are embryo lethal (Rojo et al., 2001; D'Ippólito et al., 2017). Finally, there is a shortage of both EV- and PSV-specific markers, which makes it difficult to identify the PSV unequivocally and to distinguish it from the EV or LV, particularly during developmental transitions such as embryo formation or seed germination, respectively.

Here we used a combination of experimental approaches to address the origins of PSV. We produced transgenic Arabidopsis lines expressing fluorescent protein-tagged markers for the tonoplast and the lumen of PSV, as well as tonoplast markers for pre-existing vacuoles, i.e. EV in embryos and LV in leaves. In addition, we visualised PSV using both fluorescent pH-sensitive stains and inherent PSV autofluorescence. Altogether, these markers were used to observe PSV formation in two experimental systems: embryo cells from maturing seeds and leaf cells reprogrammed toward a seed developmental program by over-expressing *LEAFY COTYLEDON2* (*LEC2*), a master regulator of seed maturation (Stone et al., 2001;

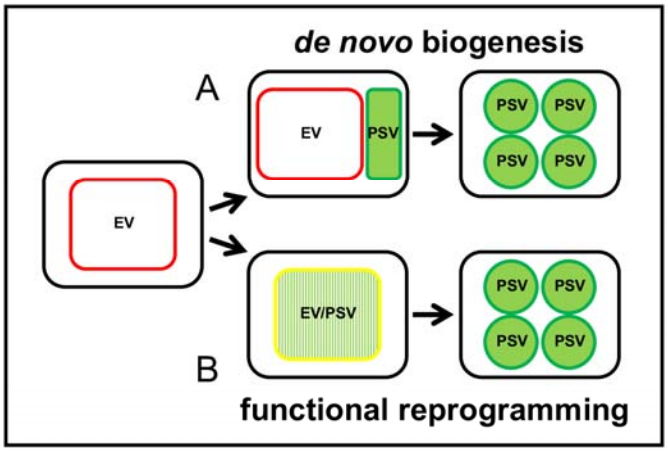

Figure 1. Hypotheses for protein storage vacuole (PSV) formation tested in this work. **(A)** PSV form *de novo*, briefly coexisting with the embryonic vacuole (EV) to eventually become the dominant structure in mature seeds. **(B)** PSV arise through reprogramming of the EV by accumulation of seed storage proteins in the EV lumen (green pattern fill). PSV-specific tonoplast markers (green outline) appear alongside the EV tonoplast markers (red outline) and coexist (yellow outline) while the EV is converted to a PSV.

Feeney et al., 2013a). These experimental systems were used to explore the two conceptually simplest scenarios of PSV formation (Fig. 1): if PSV arise *de novo*, it is likely that, as the seed matures, the newly-synthesised PSV tonoplast markers will label new compartments, which are separate from the EV. These separate compartments will contain storage proteins (Fig. 1A). If, however, PSV derive from the reprogramming of existing EV, then the PSV membrane markers will label the pre-existing tonoplast and will co-localise with the EV tonoplast markers, while storage proteins will appear in the EV lumen (Fig. 1B). We complemented these approaches with immunoelectron microscopy and serial block face scanning electron microscopy (SBF-SEM) to study vacuoles in developing embryos in 3D. Our findings indicate that Arabidopsis PSV arise by the remodelling of pre-existing EV rather than by *de novo* biogenesis of PSV.

RESULTS

Timing of PSV formation

To capture the time during development when PSV - here defined as vacuolar structures containing storage proteins - are formed, we dissected Arabidopsis embryos from developing siliques and assigned them to different stages of maturation (Fig. 2A). The stages we defined here reflect the overall morphology of the embryos after dissection from the ovule: ‘heart’ for heart-shaped embryos, ‘torpedo’ for elongated but not yet curved embryos, ‘walking stick’ for all embryos with cotyledons bent less than 90° relative to the radicle, and ‘bent cotyledon’ for all further developed green embryos (Fig. 2A). We further divided walking stick and bent cotyledon stages into early-, mid- and late- sub-stages. Mature embryos were dissected from dry seeds after imbibing them in water for approximately 3 h.

For an initial analysis of the embryo ultrastructure, embryos were fixed for transmission electron microscopy. The EV is clearly visible as a transparent structure in torpedo and walking stick embryos (Fig. 2B). However, at the early-bent cotyledon stage, electron opaque material begins to appear within the EV and this material gradually fills the vacuolar lumen in mid- and late-bent cotyledon embryos (Fig. 2B). In agreement with Mansfield and Briarty (1992), we estimate that PSV formation from an empty EV to a full PSV takes approximately 5 days. Therefore, within this time frame, we focused on the transition between late-walking stick and bent cotyledon stages, which encompasses the onset of storage protein deposition. For consistency, we chose to study cotyledon cells for both electron microscopy and live cell imaging.

During the most critical time of PSV formation, the overall morphology of the bent cotyledon embryos does not change significantly (Fig. 2). Therefore, we rely on PSV characteristics to evaluate the stage of PSV formation. Electron microscopy shows the gradual accumulation of electron opaque material in the vacuole and indicates the stage of PSV formation. Likewise, confocal microscopy of fluorescent protein-tagged tonoplast markers reveals vacuole morphologies that characterise forming PSV. With the large numbers of embryos imaged by confocal microscopy, we noted that particular events occurring during the vacuole transition could often not be pinned down to a specific developmental sub-stage, even among bent cotyledon embryos isolated from the same plant. This variability has been observed previously (Mansfield and Briarty, 1992). Consequently, for confocal analysis, we

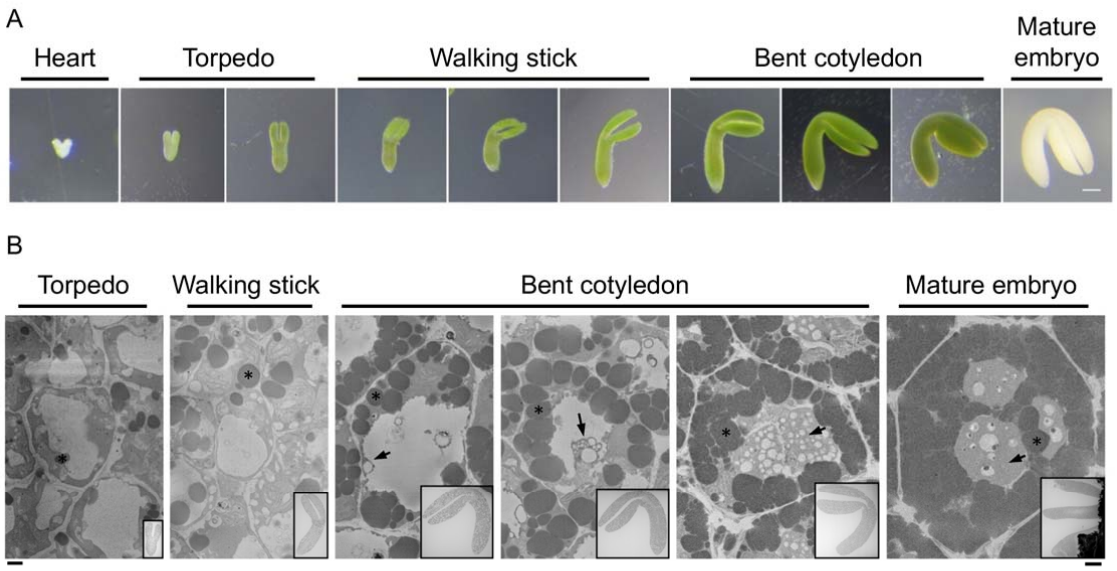

Figure 2. Stages assigned to Arabidopsis embryo development and an overview of PSV formation in a representative cell from selected stages. **(A)** Images of heart, torpedo, walking stick and bent cotyledon embryos dissected from Arabidopsis ovules. The mature embryo was dissected from a dry seed. Bar = 100 µm. **(B)** PSV arise during the maturation phase of embryonic development. Panel shows single micrographs from SBF-SEM stacks of embryos at different developmental stages. Deposits of electron opaque material (arrow) are first observed in the vacuole lumen and along the tonoplast of the EV in early-bent cotyledon embryos. The deposits accumulate and eventually fill the vacuolar lumen in mature seed. Asterisks: oil bodies. Left scale bar for high magnification images = 1 µm. Right scale bar for overview images = 100 µm.

often avoided assigning an event to a particular sub-stage of bent cotyledon embryos.

PSV tonoplast markers co-localise with tonoplast markers labelling the pre-existing EV in developing embryos

We used the temporal expression patterns of a panel of known vacuolar markers to identify, and distinguish between, the EV and PSV. As a first step to determine whether PSV are formed *de novo* or by a reprogramming of the pre-existing vacuole, we used confocal microscopy to localise two PSV-specific tonoplast proteins, the aquaporins TIP3;1 and TIP3;2 (Gattolin et al., 2011). Expression of both TIP3 isoforms is restricted to seeds and begins in bent cotyledon-stage embryos, which makes them suitable PSV markers (Johnson et al., 1990; Jauh et al., 1999; Hunter et al., 2007; Gattolin et al., 2011). To visualise the EV in late-walking stick to early-bent cotyledon embryos, we imaged the 35S-driven, expression of known tonoplast

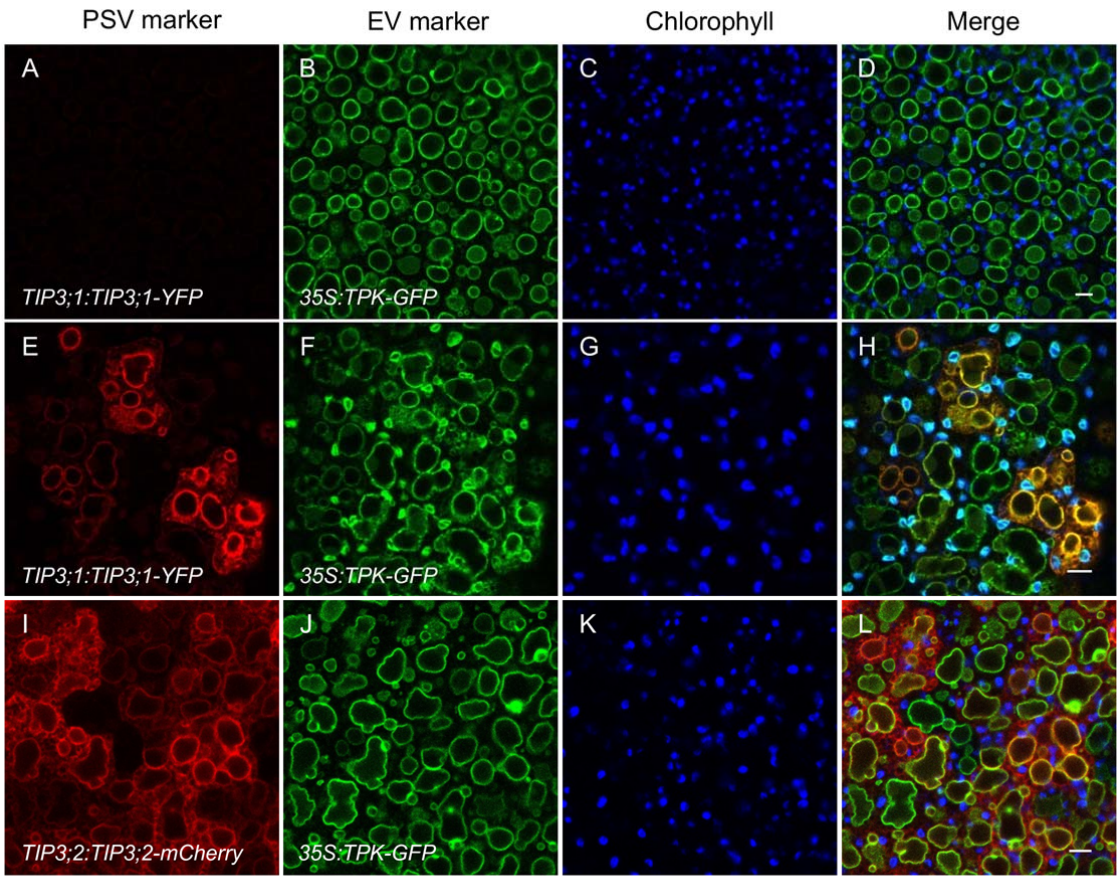

Figure 3. PSV tonoplast markers appear on the pre-existing EV tonoplast in bent cotyledon embryos. **(A-L)** Embryos constitutively expressing the tonoplast marker *35S:TPK-GFP* (green) and the PSV tonoplast markers (red) *TIP3;1:TIP3;1-YFP* (top and middle panels) or *TIP3;2:TIP3;2-mCherry* (bottom panel). Chlorophyll autofluorescence (blue). **(A-D)** In early-bent cotyledon embryos, the EV is labelled with TPK-GFP before PSV markers are expressed. **(E-L)** In later-stage bent cotyledon embryos, PSV tonoplast markers co-localise with the EV tonoplast marker. Bar = 5 μm.

proteins. These constitutively expressed markers are present on the EV tonoplast before the TIP3 PSV markers become expressed (Fig. 3A-D), thus we believe this is a viable approach to study the EV-to-PSV transition.

We imaged embryos expressing either TIP3;1-YFP or TIP3;2-mCherry, under control of their native promoters, in combination with *35S:TPK1-GFP* (Maitrejean et al., 2011) (Fig. 3). Constitutively expressed TPK1-GFP is visible in all bent cotyledon embryos and labels the EV membrane before TIP3;1-YFP or TIP3;2-mCherry markers are observed (Fig. 3A-D). Once PSV markers begin to appear, they label the same membrane as TPK1-GFP, as indicated by the co-localisation of both markers (Fig. 3E-L). It should be noted that during embryo development, chlorophyll

autofluorescence from plastids is often detectable in the GFP/YFP emission channel. To distinguish our GFP and YFP-labelled makers from plastids, a separate channel for chlorophyll autofluorescence is shown (Fig. 3C, G, K). At no stage were we able to visualise – at least at the resolution and sensitivity of the confocal microscope – separate TIP3;1-YFP or TIP3;2-mCherry-labelled structures other than the EV tonoplast.

Seed storage proteins accumulate in the EV lumen in developing embryos

If the PSV tonoplast markers localise to the EV membrane, we then hypothesised that seed storage proteins would also accumulate in the lumen of the vacuole labelled by both EV and PSV tonoplast markers. We therefore studied an Arabidopsis line co-expressing TIP3;2-mCherry and the seed storage protein 2S1 albumin fused to GFP (2S1-GFP), both driven by their endogenous promoters. When first detectable in bent cotyledon embryos, 2S1-GFP is located both in punctate structures in the cytosol and within the lumen of the existing vacuoles (Fig. 4A-D). At the same time, the TIP3;2-mCherry signal labels the tonoplast but also the ER and the plasma membrane, as previously observed (Gattolin et al., 2011). We reasoned that the 2S1-GFP punctate structures could be prevacuolar compartments/multivesicular bodies (PVC/MVB) on account of their size and distribution, as previously described (Miao et al., 2008). Staining with FM4-64 can be used to study membrane trafficking events in plant cells. The dye inserts into the outer leaflet of the plasma membrane and is thought to enter the secretory pathway by endocytosis (Bolte et al., 2004). As FM4-64 is endocytosed, it is transported to the *trans*-Golgi network/early endosome where it is sorted to the MVB (Tse et al., 2004; Dettmer et al., 2006; Ebine et al., 2008; Viotti et al., 2010) along with newly synthesised proteins, such as 2S albumins (Otegui et al., 2006; Miao et al., 2008). MVB then fuse with the vacuole to release their contents (Otegui et al., 2006; Ebine et al., 2008; Scheuring et al., 2011). Long-term staining of embryos with FM4-64 revealed localisation of 2S1-GFP-labelled punctate structures to subdomains of larger structures labelled by FM4-64 (Supplemental Fig. S1A). Using the high-resolution Zeiss Airyscan detector, the FM4-64-stained structures that associated with the punctate 2S1-GFP signals appeared brighter than other cellular structures (Supplemental Fig. S1A). Additionally, 2S1-GFP puncta no longer associating with the FM4-64 stained structures were observed to accumulate inside vacuolar lumina

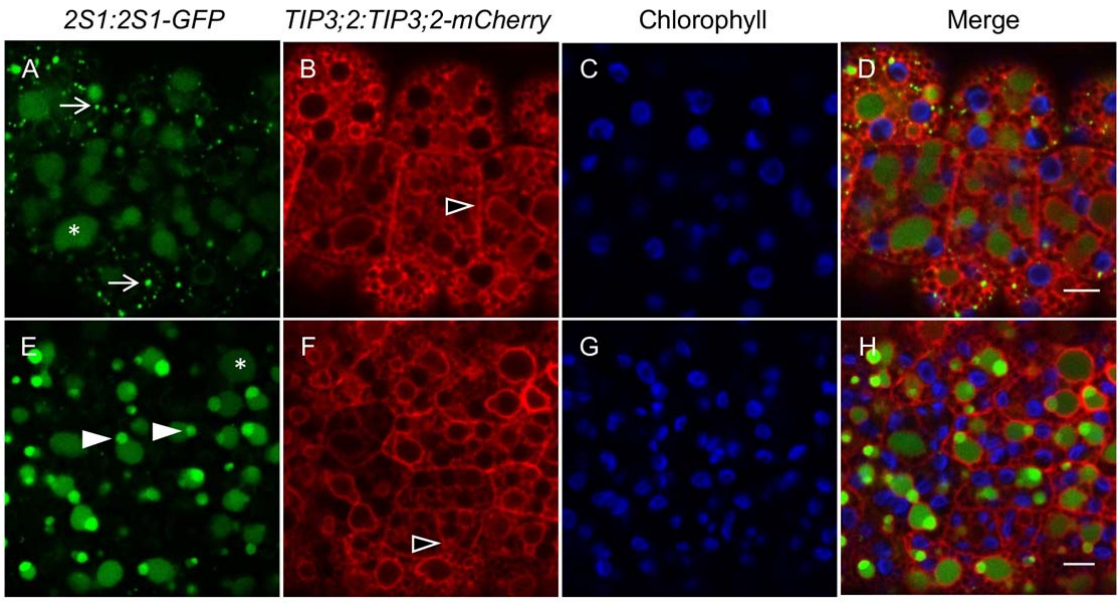

Figure 4. 2S1 albumin seed storage proteins begin to accumulate in punctate cytosolic structures and ultimately as deposits inside lumina of forming PSV in bent cotyledon embryos. **(A-H)** 2S1-GFP (green) labels small punctate structures (arrows) and accumulates in the EV/PSV lumen (asteriks). The PSV tonoplast marker TIP3;2-mCherry (red) is localised to the ER, tonoplast and also the plasma membrane (empty arrowheads). Chlorophyll is shown in blue. **(A-D)** 2S1-GFP signal is first observed as small punctate structures in the cytoplasm and accumulates in PSV lumina whose tonoplasts are labelled with TIP3;2-mCherry. **(E-H)** In late-bent cotyledon embryos, the 2S1-GFP signal is observed only in vacuole lumina. Sub-regions of more intense 2S1-GFP fluorescence are visible in PSV lumina (arrowheads). Bar = 5 µm.

(Supplemental Fig. S1B), implying that the 2S1-GFP cargo was delivered to the vacuole. At no point were the 2S1-GFP puncta seen to fuse or accumulate into a separate compartment other than EV lumina. Taken together, these observations suggest that the 2S1-GFP puncta that associate with larger FM4-64 labelled structures are likely to be PVC/MVB.

In late-bent cotyledon embryos of the Arabidopsis line co-expressing TIP3;2-mCherry and 2S1-GFP, the TIP3;2-mCherry signal becomes more visible on the tonoplast while 2S1-GFP no longer labels punctate structures and is only observed within the lumina of vacuoles (Fig. 4E-H). Within the vacuoles, sub-regions of more intense 2S1-GFP signal are observed (Fig. 4E-H, arrowheads). We were also able to observe the combined arrival of a PSV tonoplast marker and luminal marker to the EV in a triple transgenic line where the EV was labelled by *35S:TIP1;1-RFP* (Supplemental Fig. S2). In agreement with our previous results (Fig. 3E-L), EV

(TIP1;1-RFP) and PSV (YFP-TIP3;1) tonoplast markers located on the same membrane (Supplemental Fig. S2). At the same time, the PSV luminal marker (2S1-GFP) localised to the lumen of vacuoles labelled with both PSV and EV markers. Taken together, our fluorescent protein-tagged PSV markers consistently associate with the vacuole labelled by our EV markers, suggesting that PSV originate from the pre-existing EV.

PSV autofluorescence and pH-sensitive fluorescent dyes are detected within the EV

Due to the limited choice of markers available to label EV and PSV, we took advantage of the PSV's affinity for staining with pH-sensitive fluorescent dyes (Hara-Nishimura et al., 1987; Otegui et al., 2006; Gattolin et al., 2011) and their inherent luminal autofluorescence (Fuji et al., 2007; Hunter et al., 2007; Feeney et al., 2013b) to map the formation of PSV. Bent cotyledon embryos were stained with two acidotropic dyes: neutral red (NR) and BCECF-AM. At neutral pH, these stains pass freely through membranes in their unprotonated forms but protonation in acidic compartments reduces their permeability and leads to their accumulation (Dubrovsky et al., 2006; Scheuring et al., 2015).

Both stains accumulated and fluoresced within vacuoles, or sub-regions of the vacuoles whose tonoplasts were labelled with constitutively expressed TPK1-GFP and VHA-a3-RFP (Fig. 5A-H). PSV autofluorescence is observed to correlate with the staining patterns (Fig. 5, panels C, G, K). To investigate whether the staining patterns are associated with the accumulation pattern of seed storage proteins, bent cotyledon embryos expressing 2S1-GFP were stained with NR. We observed the 2S1-GFP signal to disperse within the entire vacuole lumen (Fig. 5I-L), as also shown in Fig. 4. However, bright areas of NR stain and PSV autofluorescence were both observed to co-localise with areas of more intense 2S1-GFP fluorescence in sub-regions of the vacuoles (Fig. 5I-L). These intensely fluorescent 2S1-GFP sub-regions were also seen without NR staining, as shown in Fig. 4.

To further investigate the pattern of staining and occurrence of PSV autofluorescence, bent cotyledon embryos expressing the PSV-specific tonoplast marker YFP-TIP3;1 under its native promoter were stained with NR. As PSV form from the large, round EV (Supplemental Fig. S3A) and remodel to assume the characteristic mature PSV morphology (Supplemental Fig. S3B-C), NR staining

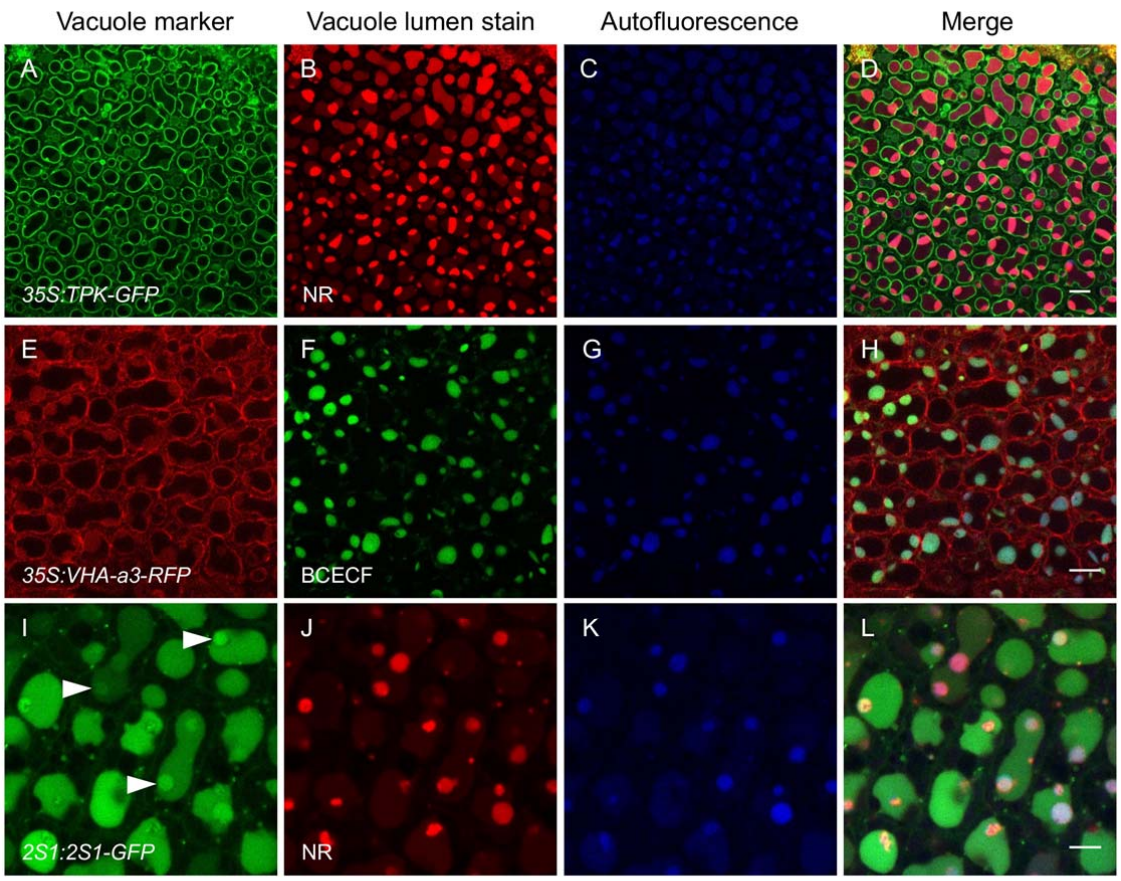

Figure 5. Forming PSV are identified by the acidotropic stains NR and BCECF-AM as well as PSV luminal autofluorescence in bent cotyledon embryos. **(A-H)** NR and BCECF-AM stain vacuoles labelled with the tonoplast markers TPK-GFP **(A)** or VHA-a3-RFP **(E**), respectively. Vacuole lumen autofluorescence (blue) co-localises with the stains **(D, H)**. **(I-L)** Embryos accumulating 2S1 albumin-GFP were stained with NR. The 2S1-GFP signal fills vacuole lumina and areas of more intense GFP fluorescence are observed (arrowheads) **(I)**. NR stains distinct sub-regions of vacuole lumina **(J)**. These NR-stained sub-regions co-localise with PSV lumen autofluorescence **(K)** and to areas of intense 2S1-GFP fluorescence **(L)**. Bar = 10 µm **(A-H)** and 5 µm **(I-L)**.

becomes more prominent. The stain initially accumulates in discrete zones within the vacuolar lumen (Supplemental Fig. S3A), to then eventually stain the entire lumen in late-bent cotyledon embryos (Supplemental Fig. S3C). At no point are the stains observed to accumulate in structures other than vacuoles labelled by EV (Fig. 5A-H) or PSV (Supplemental Fig. S3) tonoplast markers. A similar pattern is observed for PSV autofluorescence in forming PSV (Supplemental Fig. S3D-F). Taken together, these data indicate that the accumulation of both acidotropic stains and inherent PSV autofluorescence correlates with the EV reprogramming to become the PSV.

PSV tonoplast markers and seed storage proteins label a transitioning EV

Our light microscopy observations were corroborated by immunoelectron microscopy to identify where PSV marker proteins begin to accumulate. For embryos prepared for immunogold labelling, the EV is characterised by a large, translucent lumen in torpedo, walking stick and early-bent cotyledon stage embryos (Fig. 6, panels A, C, E). However, unlike routine EM (Fig. 2B), specimens for immunogold labelling were not fixed with osmium. Oil bodies (which, due to lack of osmium in this preparation, also appear translucent) were differentiated from the EV by their rather uniform size, round shape and the lack of flocculent material in the lumen.

Antibodies against TIP3;1 as well as 2S albumin and 12S globulin seed storage proteins showed no significant gold labelling in embryos from heart to walking stick stages (Supplemental Fig. S4). In early-bent cotyledon embryos, anti-TIP3;1 antiserum labelled the tonoplast of the large, translucent EV (Fig. 6A) and anti-2S and anti-12S were detected along the inner periphery of the tonoplast and on electron opaque material within the lumen of the vacuole (Fig. 6C, E). In late-bent cotyledon embryos, the lumen of the maturing PSV is completely filled with electron opaque material (see also Fig. 2B) and shows a high density of gold labelling with anti-TIP3;1, anti-12S and anti-2S antibodies (Fig. 6, panels B, D, F). To allow a quicker visualisation of the distribution of the gold particles we highlighted them on transparent versions of the micrographs (Supplemental Fig. S5). These results support our confocal microscopy observations that suggest that TIP3 isoforms and seed storage proteins appear at the tonoplast and in the lumen of the EV, respectively (Fig. 4, Supplemental Fig. S5).

In addition, the electron opaque material accumulating along the periphery and dispersed within the EV/PSV lumen was labelled by anti-complex glycan antiserum (Lauriere et al., 1989), confirming that at least a proportion of PSV glycoproteins underwent N-glycan processing in the Golgi (Supplemental Fig. S6).

PSV form by a remodelling of the LV in leaf cells reprogrammed by LEC2

Our data so far indicate that in embryos the PSV is formed by the repurposing of the pre-existing vacuole. In order to test whether this functional transition could be recapitulated in a system where the only vacuole present is the LV, we investigated the formation of PSV in leaves reprogrammed to follow a seed developmental pathway by the over-expression of *LEC2* (Feeney et al., 2013b). *LEC2* is a key

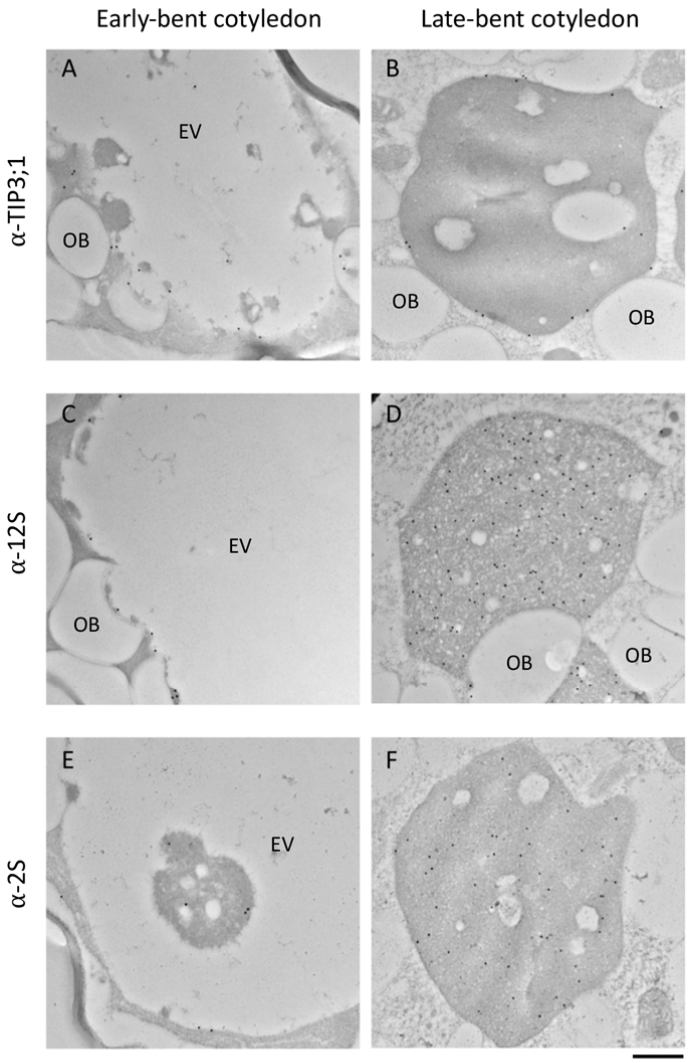

Figure 6. The PSV tonoplast aquaporin TIP3;1 as well as the 2S albumin and 12S globulin seed storage proteins are localised to the EV by immunogold labelling in bent cotyledon embryo cells. **(A-B)** Anti-TIP3;1 antibody labels the tonoplast of transitioning vacuoles. **(C-D)** Anti-12S globulin antibody labels electron opaque material accumulating along the luminal side of the tonoplast **(C)** and the entire PSV lumen in late-bent cotyledon embryos **(D)**. **(E-F)** Anti-2S antibody labels electron opaque material accumulating along the luminal side of the tonoplast **(E)** as well as electron opaque material in the vacuole lumen **(F)**. Oil bodies (OB). Bar = 500 nm.

295 transcriptional regulator of seed development and, when over-expressed in

296 vegetative tissues, causes cells to change their developmental pathway and acquire

297 characteristics of maturation phase embryos. We previously showed that, in this

298 system, leaf LV are replaced by PSV (Feeney et al., 2013a). The details of the LV-to-

299 PSV transition were however not explored. Therefore, with a similar strategy to that

used for embryos as described above, we imaged leaf cells of Arabidopsis

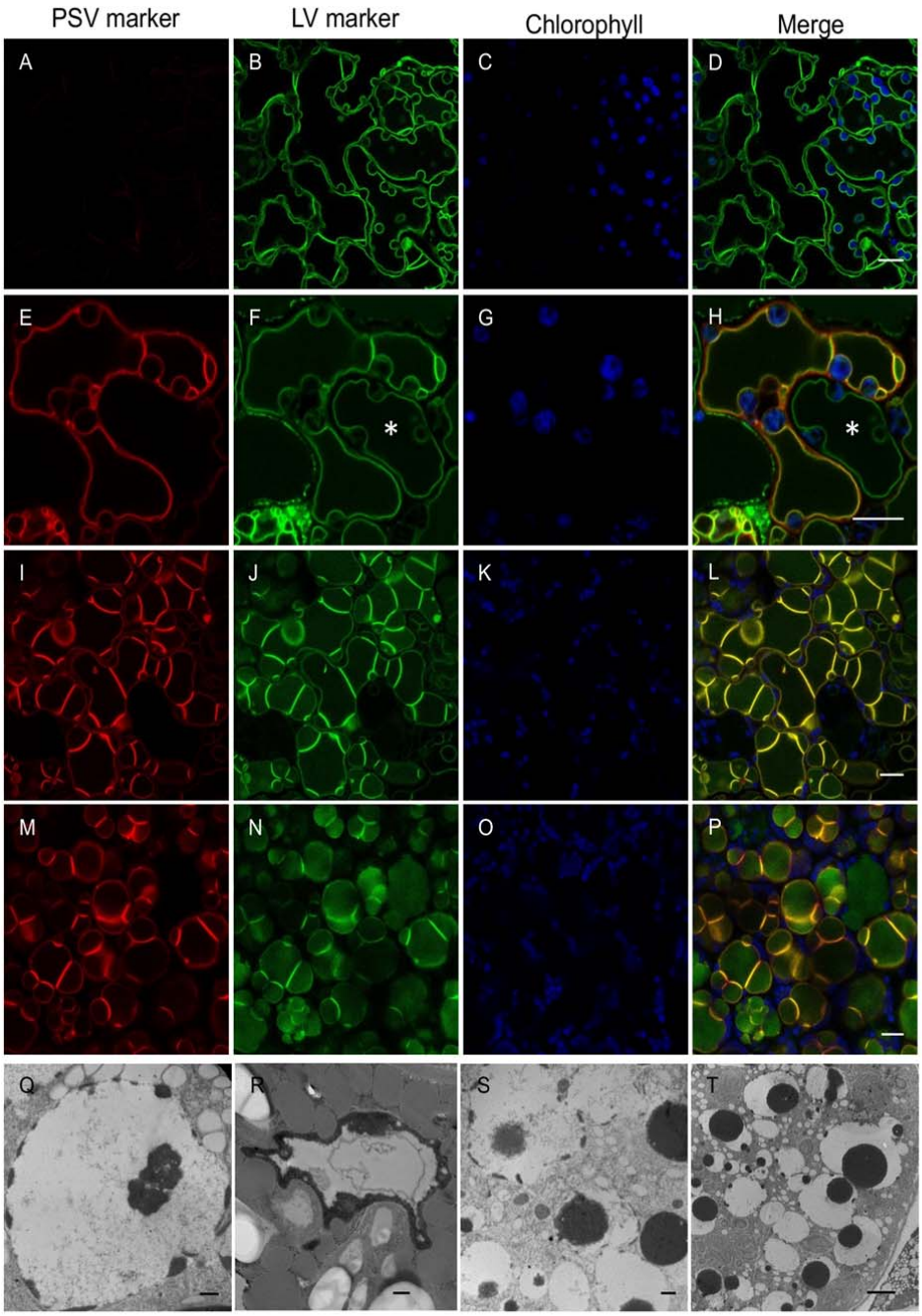

Figure 7. PSV form by a remodelling of the LV in Arabidopsis leaf cells reprogrammed by LEC2. **(A-P)** Representative images of transitioning vacuoles in LEC2-induced leaf cells at 14 **(A-D)**, 17 **(E-H)** and 20 **(I-P)** days on DEX. The TIP3;1-YFP PSV tonoplast marker (red) accumulates on the pre-existing LV **(E, I, M)** in Arabidopsis lines constitutively expressing the tonoplast marker TPK-GFP (green). Chlorophyll autofluorescence is shown in blue. Asterisk shows asynchronous remodelling of tonoplast in neighbouring cells. Bar = 10 µm. **(Q-T)** Electron microscopy of leaf cells 14 days after LEC2 induction with DEX. Electron opaque PSV material (black) accumulates along the luminal side of the tonoplast and disperses in the vacuole lumen. Bar = 500 nm **(Q-S)** and 2 µm **(T)**.

301 *35S:LEC2-GR* lines where the LV was labelled with a constitutively expressed

tonoplast marker, TPK1-GFP, and observed the localisation of the PSV marker TIP3;1-YFP, expressed under its native, seed-specific promoter (Fig. 7A-P). At 14 days on dexamethasone (DEX) to induce *LEC2* over-expression (Fig. 7A-D), the PSV marker is not yet detectable while the TPK-GFP marker labels the LV tonoplast. Between 15-20 days on DEX, the PSV marker becomes detectable and is observed to co-localise to the LV marker on the same tonoplast (Fig. 7E-P), indicating that the LV is reprogrammed to become a PSV. During the LV-to-PSV transition, leaf LV morphology changes from a large central compartment that mirrors the cell's shape (Fig. 7A-D) to smaller vacuoles that are more round in shape, resembling PSV (Fig. 7M-P). In addition, the images show asynchronous remodelling of tonoplast in neighbouring cells; LV highlighted solely with TPK1-GFP lack tonoplast folds (Fig. 7E-H, asterisk). However, adjacent vacuoles accumulating both TPK1-GFP and TIP3;1-YFP possess brightly fluorescent tonoplast folds, as reported in (Feeney et al., 2013a; Feeney et al., 2013b).

In a similar manner to developing embryos, LEC2-induced leaf cells accumulate PSV material in the LV/PSV (compare Fig. 7Q-T with Fig. 2B and Fig. 6). Transmission electron microscopy of leaf cells from *35S:LEC2-GR* plants grown in the presence of DEX for 14 days provides a representation of the LV-to-PSV transition (Fig. 7Q-T). Electron opaque material accumulates along the inner periphery of the LV tonoplast and is observed to disperse within the vacuole lumen. These electron opaque deposits were previously shown to contain 12S globulin and 2S albumin seed storage proteins by immunogold labelling (Feeney et al., 2013a).

The LV-to-PSV transition occurs over approximately 5 days in LEC2-induced leaf cells, as shown in Fig. 7. To visualize the highly dynamic nature of the vacuole remodelling occurring over this time course, optical sections were taken through leaf cell vacuoles of LEC2-induced plants harbouring *35S:TPK1-GFP*. Maximum intensity projections of representative images are shown in Fig. 8. At approximately 14 days on DEX, LV appear normally shaped (Fig. 8A) but possess more transvacuolar strands than control leaf cells without DEX (Fig. 8F). However, as the LV transitions to a PSV, the tonoplast undergoes extensive remodelling (Fig. 8B-D). At approximately 20 days on DEX, vacuoles are more round in shape and resemble PSV (Fig. 8E). A time series taken from a representative cell during this transition stage reveals fast tonoplast remodelling, compared to minimal remodelling in non-induced cells (Supplemental Fig. S7 and Supplementary Movies 1 and 2).

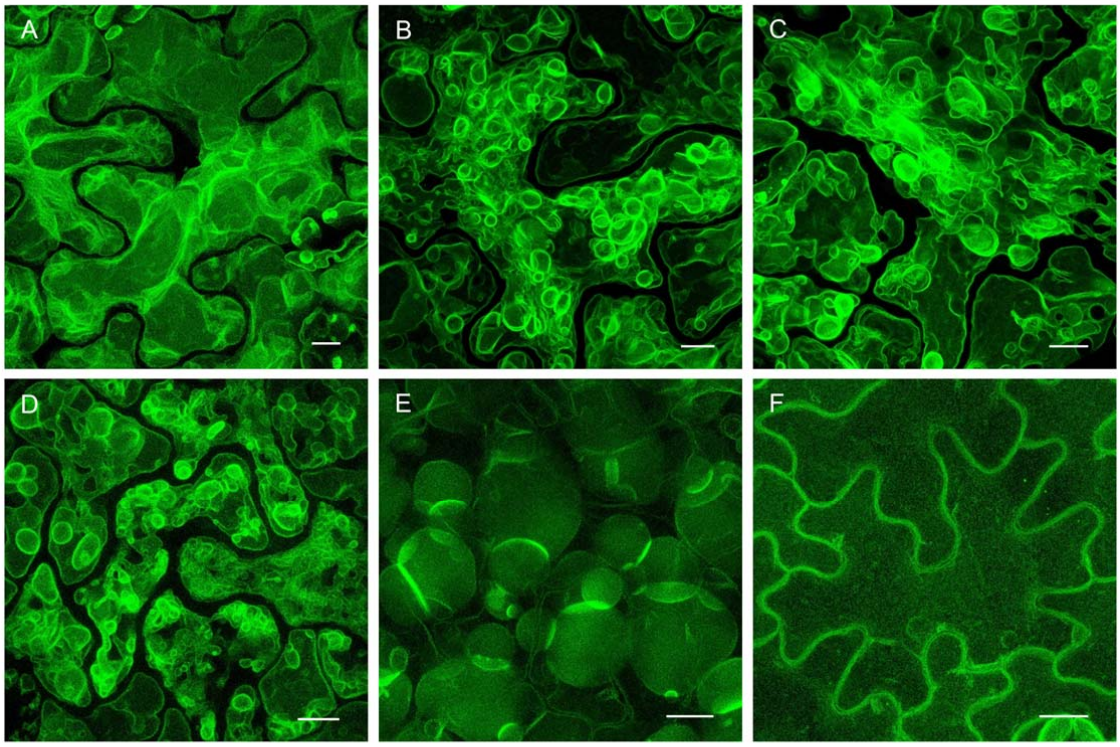

Figure. 8. Tonoplast undergoes extensive remodelling during the LV-to-PSV transition in LEC2-induced leaf cells. **(A-F)** Representative images showing the progression of tonoplast remodelling during the LV-to-PSV transition at 14 **(A)**, 17 **(B, C)**, and 20 **(E)** days on DEX, or on 14 days without DEX **(F)**. Arabidopsis *35S:LEC2-GR* lines harbouring *35S:TPK1-GFP* (green) were imaged. Images are maximum intensity projections of Z-stacks taken through leaf epidermal cells. Bar = 10 µm.

336

337 ***PSV formation involves extensive remodelling of the EV***

Embryo cells contain one large EV at the torpedo stage. However, in mature embryo cells, there appear to be multiple, smaller PSV present (Fig. 2B). To better understand the EV-to-PSV transition, we used SBF-SEM to obtain 3D datasets of embryos at different developmental stages. By serially imaging the block faces cut at 100 nm intervals through whole cells with high resolution SEM, we were able to acquire image stacks of entire cells and reconstruct the entire vacuolar system in developing embryos. For comparison, we chose cells in the cotyledon tip of embryos from torpedo, early-, mid- and late-bent cotyledon stages and from a mature seed (Supplemental Fig. S8). We reconstructed the translucent lumen of the EV, electron

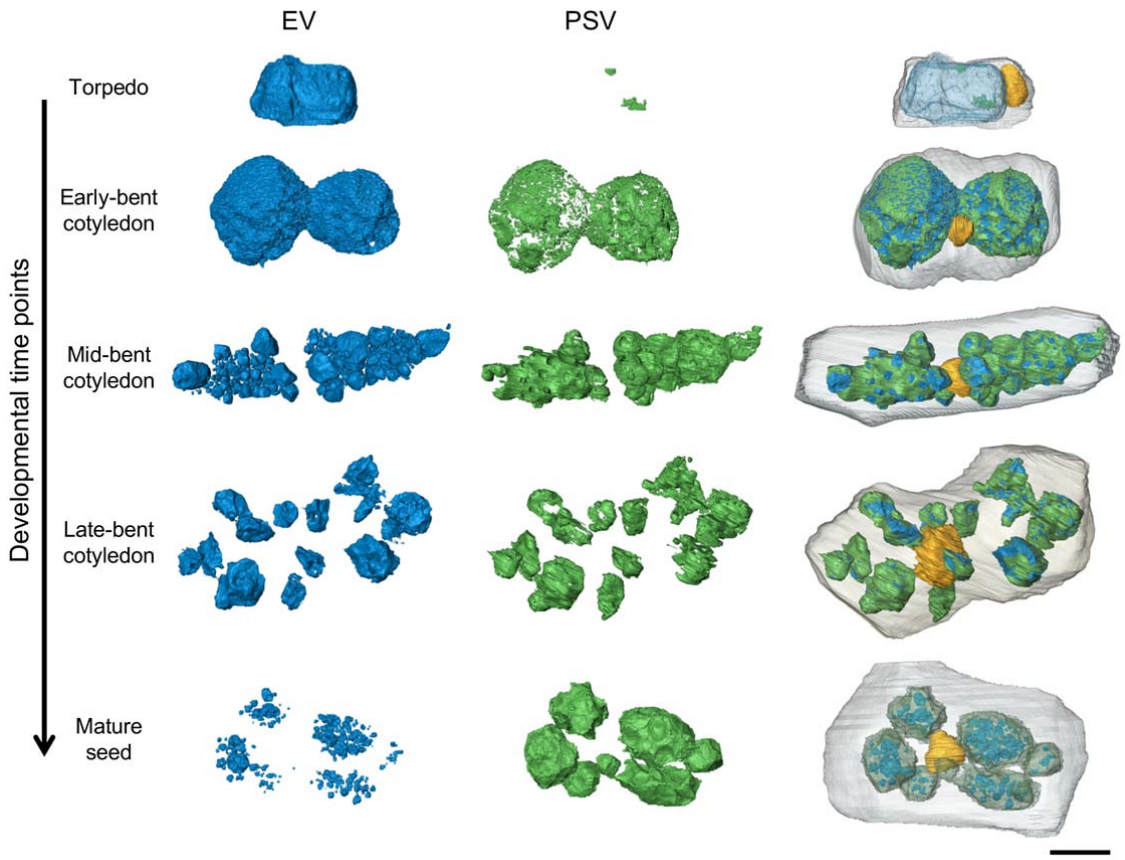

Figure 9. Remodelling of the EV to PSV during embryo maturation. The lumen of the EV (blue), electron-opaque PSV luminal material (green), nucleus (yellow) and plasma membrane (grey) were rendered from SBF-SEM image stacks in cotyledon cells of embryos in the torpedo, early-, mid- and late-bent cotyledon or mature embryo stages. As electron-opaque material initially accumulates along the periphery of the EV lumen, the vacuole separates into several smaller vacuoles which are eventually filled with electron-opaque PSV luminal material aside from small remains. The nucleus changes position from the cell cortex to the centre of the cell. Bar = 5 µm.

opaque PSV material composed of seed storage proteins (according to our antibody labelling; Fig. 6), the nucleus and the cell membrane (Fig. 9). For the original datasets and animated reconstructions see Supplemental Movies 3-10.

During seed maturation, storage proteins (Fig. 9, green) increasingly accumulate along the periphery of the EV lumen (Fig. 9, blue) and take up an increasing proportion of the vacuolar volume (Supplementary Fig. S9). At the same time the large EV divides into smaller vacuoles which are eventually filled with storage protein. In the mature seed, the EV has been replaced by multiple PSV. Electron opaque PSV lumina possessed small, translucent and partly crystalline

356 inclusions (Fig. 2B, Supplemental Fig. S9). These inclusions are often identified as
357 globoids (Jiang et al., 2001). To maintain consistency in our reconstructions, these
358 translucent inclusions were considered to be EV (Fig. 9, Supplemental Fig. S9),
359 though we are unable to speculate on their ontology. Additionally, as the embryo
360 matures the nucleus changes position from the cortex to the centre of the cell (Fig. 9,
361 yellow). These snapshots of PSV formation during embryo development captured in
362 3D using SBF-SEM provide further evidence that the PSV originates from the pre-
363 existing EV.
364
365

DISCUSSION

Our data provide a dynamic picture of PSV formation during seed maturation and indicate that in Arabidopsis embryo cells, PSV do not arise *de novo* but result from the repurposing of the pre-existing EV. While it has been previously reported that mature seeds only appear to contain PSV (Otegui et al., 2006; Hunter et al., 2007), the events leading to the formation of PSV in Arabidopsis have not previously been documented.

To establish where PSV originate in Arabidopsis embryo cells, we used lines expressing fluorescently-labelled vacuolar markers, acidotropic stains, PSV autofluorescence, high resolution Zeiss CLSM Airyscan detection, SBF-SEM and immunoelectron microscopy. According to our definition of PSV as vacuolar structures that contain seed storage proteins, our data indicate that PSV formation begins between late-walking stick and early-bent cotyledon stages (Fig. 2B).

PSV formation involves an accumulation of electron opaque material in the lumen of the pre-existing vacuole. The elemental composition of the electron opaque material accumulating in PSV has been characterised by means of energy-dispersive x-ray spectroscopy analysis by Zheng and Staehelin (2011) and Otegui et al. (2002). The principal components of the spectrum were potassium, calcium, magnesium, as well as phosphorus, which was characterised as phytate (myoinositol-hexakisphosphate). Our immunogold labelling shows that seed storage proteins (Fig. 6 and Supplemental Fig. S5) and glycoproteins that have trafficked through the Golgi (Supplemental Fig. S6) are also found within the electron opaque material. Similarly, the seed storage protein vicilin and barley lectin were detected in electron opaque material in transitioning pea and barley vacuoles (Hoh et al., 1995; Olbrich et al., 2007) as well as 12S globulins and 2S albumins in LV transitioning to PSV in leaf cells reprogrammed by *LEC2* over-expression (Feeney et al., 2013a). Zheng and Staehelin (2011) distinguished between vacuoles undergoing PSV-to-LV transitions in tobacco root meristematic cells by the presence of electron opaque PSV material using TEM. We similarly observed the appearance of electron opaque deposits during the EV-to-PSV and LV-to-PSV transitions in embryos and leaves reprogrammed by *LEC2* over-expression, respectively.

Nascent vacuolar proteins traffic from the endoplasmic reticulum to their ultimate destination in the EV/PSV. Throughout the vacuolar transition, we observed trafficking of the marker proteins. As PSV form, tonoplast markers, particularly the

TIP isoforms, are observed in the ER *en route* to the tonoplast (Fig. 4, Supplemental Fig. S2). Similarly, the seed storage protein 2S1 albumin-GFP is observed as punctate structures at its earliest time of detection (Fig. 4A-D; Supplemental Fig. S1). Seed storage proteins are sorted at the Golgi apparatus into dense vesicles that fuse with other small vesicles carrying proteolytic enzymes to give rise to PVC/MVB (Otegui et al., 2006). These organelles function as prevacuolar compartments in the secretory pathway and ultimately fuse with the vacuole (Ebine et al., 2008; Scheuring et al., 2011). Therefore, the punctate 2S1-GFP structures that we observe during early PSV formation are likely to be PVC/MVB, as previously described (Ebine et al., 2008; Miao et al., 2008).

Mature PSV can be identified by the accumulation of acidotropic fluorescent stains and PSV autofluorescence in their lumina (Fuji et al., 2007; Hunter et al., 2007; Feeney et al., 2013b), although we do not yet know what is contributing to PSV autofluorescence. We show here that NR, BCECF-AM and PSV autofluorescence can be used to identify forming PSV (Fig. 5, Supplemental Fig. S3). Within early PSV lumina, co-localisation of NR, PSV autofluorescence and 2S1-GFP fluorescence into distinct, brighter areas suggest the existence of sub-regions in the matrix of the transitioning vacuole during seed filling (Fig. 5I-L). A similar observation was made in vacuoles of developing pumpkin cotyledons stained with NR (Hara-Nishimura et al., 1987). In our study, these distinct areas were first observed to accumulate in the EV/PSV lumen as small, highly-fluorescent regions that increased in volume, eventually filling the PSV lumen (Supplemental Fig. S3). Looking at cross sections of our 3D SBF-SEM datasets, we can sometimes observe a similar accumulation of electron opaque material in one area of the EV, potentially representing such a sub-region (Supplemental Fig. S9, early-bent cotyledon). It will be interesting to explore the nature of these EV/PSV sub-regions and how they relate to the biogenesis of the PSV as a compound organelle (Jiang et al., 2000; Jiang et al., 2001).

Once we understood that PSV originate from EV in developing embryos, we documented how a single EV, occupying nearly the entire cell volume, transitions to become a collection of numerous, smaller-sized PSV within the mature embryo cell. SBF-SEM allowed us to image the entire embryo to visualise the 3D organization of cells and tissues and, likewise, the spatial organisation of vacuolar structures in those cells. Reconstructions from SBF-SEM data of cotyledon cells from one embryo

each of torpedo, early-, mid- and late-bent cotyledon stages and a mature embryo (Fig. 9 and Supplemental Fig. S9) provide snapshots of how EV remodel to form PSV. In mature seeds, PSV exist as a group of separate, individual entities that do not appear to form an interconnected network, as previously suggested by light microscopy data (Hegedus et al., 2015).

The biogenesis of PSV has been a long-standing topic of debate. In cotyledon cells of developing pea embryos, an accumulation of electron opaque material was observed within a tube-like, membrane-bounded structure surrounding the EV during embryo development in pea. PSV and EV membranes were labelled with anti-TIP3;1 and anti-TIP1;1 antibodies, respectively (Hoh et al., 1995). Altogether, these results supported a *de novo* mechanism for PSV development. Therefore, if nascent PSV arise separately from the pre-existing vacuole, we may anticipate their respective tonoplasts to possess unique TIP isoform markers and, more importantly, seed storage proteins should accumulate in the lumen of the PSV and not within the lumen of the pre-existing vacuole. Others have reported TIP1;1-labelled internal membranes in PSV lumina (Gillespie et al., 2005; Bolte et al., 2011). In Arabidopsis embryos, however, we were unable to detect TIP1;1 accumulation on the EV tonoplast (data not shown) and our EV and PSV tonoplast markers appear to co-localise on the same EV membrane (Fig. 3). This is in agreement with previous results in Arabidopsis embryo cells (Otegui et al., 2006; Gattolin et al., 2011) and in PSV forming in leaf cells reprogrammed by LEC2 (Feeney et al., 2013a). Moreover, we consistently observe seed storage proteins accumulating in the lumen of the vacuole labelled by both EV and PSV tonoplast and luminal markers. Therefore, we reason that in Arabidopsis PSV arise by a remodelling of the pre-existing vacuole.

In Arabidopsis, the presence of adjacent tonoplasts in embryo vacuoles was observed in single sections (Frigerio et al., 2008), potentially suggesting the presence of separate vacuoles. The present study, which covers several developmental time points during PSV biogenesis across whole cellular volumes, shows that extensive membrane remodelling occurs during seed maturation. It is therefore possible that the multiple membranes observed at a fixed point may reflect tonoplast remodeling rather than the presence of a separate structure. Upon close inspection of our TEM data, we did not observe a membrane surrounding the storage proteins aggregates forming in bent cotyledon embryos or transitioning vacuoles of LEC2-induced leaf cells (Supplementary Fig. S10). In both cases, the

tonoplast appears as a clearly defined interface surrounding the outer periphery of the protein aggregates. However, the inner periphery of these aggregates, which faces the vacuole lumen, appears fuzzy and poorly defined, which does not suggest that it is membrane-bounded. In addition, immunolabeling of transitioning LEC2-induced leaf vacuoles with an anti-TIP3;1 antiserum shows that the PSV membrane does not enclose the seed proteins but is solely localised to the tonoplast of the pre-existing LV (Feeney et al., 2013a; Supplementary Fig. S10). Therefore, our results do not support the hypothesis that the PSV arise by a *de novo* structure but more strongly support a remodelling mechanism for PSV biogenesis.

This work provides a foundation to further explore the mechanism of PSV biogenesis. During the EV-to-PSV transition, it will be interesting to understand how the EV lumen environment changes to accommodate the influx of seed storage proteins. The over-expression of seed storage proteins targeted to the leaf LV results in degradation of the proteins (Bagga et al., 1992; Frigerio et al., 1998; Frigerio et al., 2000), however reprogramming of the LV to a PSV alters the luminal environment to accommodate incoming storage proteins (Feeney et al., 2013a). While it is established that storage proteins are delivered to the nascent PSV by fusion of MVB (Otegui et al., 2006), additional processes must be at play.

That PSV can arise from both the EV and LV raises some general questions about the relationship between the EV and LV. During the evolution of seed plants, the maturation phase was integrated into embryogenesis to enable plants to interrupt their life cycle (Vicente-Carbajosa and Carbonero, 2005). A network of transcriptional regulators, such as *LEC2*, are responsible for regulating the activities occurring during this developmental phase (Braybrook and Harada, 2008; Baud et al., 2016), including the formation of PSV (Feeney et al., 2013a; Feeney et al., 2013b). In lower plants, there is no separation between embryo morphogenesis and post-embryonic development (West and Harada, 1993). Altogether, this suggests that the evolution of seeds has commandeered the existing cellular structures and that perhaps the EV and LV are the same vacuole but accommodate a different complement of proteins.

In conclusion, our analysis of the early stages of PSV formation in Arabidopsis suggests that, rather than by a *de novo* process, PSV arise by functional reprogramming of the EV. While we do not attempt here to elucidate *how* this change happens, our findings pave the way to understanding the processes underpinning such a developmental change.

502

503

METHODS

Plant materials

Arabidopsis thaliana lines used in this study for confocal microscopic analysis were Col-0, or lines harbouring *35S:TPK1-GFP* (Voelker et al., 2006; Maitrejean et al., 2011), *35S:VHA-a3-mRFP* (Brux et al., 2008), *TIP3;1:TIP3;1-YFP/TIP1;1:TIP1;1-RFP*, *TIP3;1:YFP-TIP3;1*, *TIP3;2:TIP3;2-mCherry* (Gattolin et al., 2009; Gattolin et al., 2011), *35S:LEC2-GR* (Stone et al., 2008). The 2S1 albumin marker line *2S1:2S1-GFP* was modified from (Miao et al., 2008). The *2S1-GFP* fusion from vector pBI221 (Miao et al., 2008) was PCR amplified with *BamH*I and *EcoR*I restriction sites and the product was ligated into binary vector pCaMterX (Harris and Gleddie, 2001). The 2S1 promoter region was cloned from Col-0 genomic DNA by amplifying 914 bp upstream of the *2S1 albumin* coding sequence (At4g27140) with the addition of *Cla*I and *BamH*I restriction sites. The *35S* promoter was excised from pCaMterX by cutting with *Cla*I and *BamH*I and was replaced with the *2S1 albumin* promoter region. For experiments, crosses were made for combinations of the above marker lines. For EM studies, Col-0 plants or Ws-0 plants harbouring the *35S:LEC2-GR* construct (Stone et al., 2008) were used.

Tissue culture conditions and LEC2 induction

Sterilized seeds were transferred to germination medium consisting of Murashige and Skoog (MS) salts (Sigma) supplemented with full strength MS vitamins and 0.4 mg/L thiamine-HCl, 100 mg/L myo-inositol, 30 g/L sucrose and 0.75% agar, pH 5.8. Seeds were stratified for 3-4 days at 4°C in the dark and transferred to a growth chamber for germination. The growth chamber was set at 24°C day/ 22°C night with 70 µmol/m^2/sec irradiance and with a 16 h light/ 8 h dark photoperiod.

To induce *LEC2* over-expression, stratified seeds were allowed to germinate and grow for 7 days on germination medium. Seedlings were then transferred to induction medium composed of MS germination medium supplemented with 30 µM dexamethasone (DEX; Sigma-Aldrich). DEX was solubilized in DMSO. Seedlings were incubated on DEX for up to 21 days before imaging.

Greenhouse growth conditions and embryo isolation from siliques

Seedlings germinated in tissue culture were transferred to soil and grown at 20°C day/ 18°C night with a minimum of 178 µmol/m^2/sec irradiance and with a 16 h light/

8 h dark photoperiod for approximately 6 weeks. For confocal imaging, one flower stalk was selected for each line. Siliques (8-12) were harvested from the mid- to lower- region of the flower stalk, closest to the rosette. Using a stereomicroscope, ovules were dissected from siliques and transferred to a 1.5 ml tube. A pestle was used to gently squash the ovules to release embryos. The plant material was then transferred to a Petri dish filled with water. Embryos were gently separated from the debris and were classified and sorted according to their developmental stage as described in the results and shown in Fig. 2A.

Fluorescence and confocal laser scanning microscopy and staining

Seeds and seedlings were screened for fluorescence using a Leica MZ FLIII fluorescence stereomicroscope. To observe GFP and YFP fluorescence, a standard GFP filter (excitation BP480/40 nm; emission, LP510 nm) was used. To observe RFP fluorescence, an RFP filter (excitation 546/10 nm; emission, LP590 nm) was used.

For confocal microscopy, embryo and leaf samples were directly observed or stained before examination with a Zeiss CLSM880. All imaging was performed on embryo cotyledon cells. To stain vacuole lumina, embryos were stained for 5 min with 17.5 µM NR (Sigma) or for 30 min with 10 µM BCECF-AM (Molecular Probes). Embryos were washed 3 times with water before imaging. For long-term staining with FM4-64, embryos were incubated for 1 h in 8 µM FM4-64, washed three times with water and incubated for a further 2.5-3 h in water before imaging. Confocal imaging was performed using a 63x (1.4 NA) oil immersion lens. A 405 nm laser line was used to visualise PSV autofluorescence and 440-490 nm emission was collected. A 488 nm laser line was used to excite GFP and BCECF-AM and emissions were collected as 505-540 nm for GFP and 500-560 nm for BCECF-AM. A 514 nm laser line was used to excite YFP and FM4-64 and emissions were collected as 525-585 nm for YFP and 615-645 nm for FM4-64. A 561 nm laser line was used to excite RFP and NR and emissions were collected as 565-640 nm for RFP and 560-615 nm for NR. A 630 nm laser line was used to visualise chlorophyll autofluorescence and 645-720 nm emission was collected. Sequential detection of combinations of the above fluorophores was performed by combining their settings in the frame scanning mode. Z-stacks were recorded using optimal scan parameters. For Airyscan detection, samples were imaged using a 100x (1.46 NA) oil immersion

lens. Image processing was performed with Zeiss Zen Lite software. Temporal colour-coding of time series data was performed using FIJI software.

Immunogold labelling and transmission electron microscopy

Embryos were isolated from siliques as described above and fixed in 2.5% (v/v) glutaraldehyde and 4% (w/v) paraformaldehyde in 0.1M sodium phosphate buffer, pH 7.4 at 4°C as previously described (Feeney et al., 2013a). Embryos were dehydrated in a graded ethanol series and were then infiltrated in increasing concentrations of LR White resin. Infiltration in pure LR White resin was carried out for 3 days. In the last 24 h of infiltration, 0.5% benzoin methyl ether was added as catalyst for polymerization. Embryos were embedded in flat embedding dishes sealed with Melinex film (Agar Scientific) and polymerized under UV light at -20°C for 24 h followed by 0°C for 24 h.

Specimens were cut into 70 nm-thick sections and collected on nickel mesh grids for immunogold labelling experiments using an RMC PowerTome ultramicrotome (RMC, Tucson, Arizona). Sections were blocked with goat normal serum (Aurion) for 30 min, followed by 2 h with primary antibodies diluted with dilution buffer (0.2 [v/v] BSA-c [Aurion], 0.05% [v/v] Tween 20 and 1% [w/v] BSA in phosphate-buffered saline, pH 7.4). Primary antibodies were rabbit-anti-TIP3;1 (1:10) (Jauh et al., 1999), rabbit-anti-12S globulin (1:500) (Shimada et al., 2003), rabbit-anti-2S albumin (1:500) (Scarafoni et al., 2001) and rabbit-anti-complex glycan (1:500) (Lauriere et al., 1989). Specimens were incubated for 1 h with secondary antibodies diluted 1:10 with dilution buffer. All secondary antibodies were IgGs produced in goats and conjugated to 15 nm gold particles (Aurion). All specimens were stained for 30 min with 4% (w/v) uranyl acetate (UA) and 20 min with lead citrate (Reynolds, 1963) followed by 3 min with 4% (w/v) UA. Specimens were examined with an Hitachi H-7650 transmission electron microscope operating at 100 kV.

Leaves were collected from LEC2-induced plants and were fixed, infiltrated and embedded in LR Gold resin according to (Feeney et al., 2013a). Specimens were cut into 60 nm-thick sections and stained for 10 min with 5% (w/v) UA and 1 min with lead citrate (Feeney et al., 2013a) and were examined with a CM-10 transmission electron microscope (Philips) operating at 80 kV.

606 **Serial block face scanning electron microscopy**

607 Embryos were isolated as described above and fixed in 1% (v/v) glutaraldehyde and
608 1% (w/v) paraformaldehyde with 2% sucrose and 2 mM $CaCl_2$ in 0.1M sodium
609 cacodylate (NaCac) buffer, pH 6.9 for 60 min at room temperature. Embryos were
610 washed in NaCac buffer, then incubated in 1% tannic acid in 0.1M NaCac buffer for
611 60 min. Embryos were washed with water 3 x 10 min, stained in 1% aqueous
612 osmium tetroxide for 2 h at room temperature, then washed in deionised water and
613 dehydrated in a graded ethanol series. Embryos were then infiltrated in gradually
614 higher concentrations of Spurr resin. Infiltration with pure resin was carried out for 3
615 days with resin replaced every 24 h. Embryos were embedded in flat dishes and the
616 resin polymerized at 70°C for 12 h. Embryos were mounted onto SBF-SEM stubs
617 with conductive adhesive resin as previously described (Kittelmann et al., 2016).
618 Trimmed blocks were gold sputter coated for 30 sec (~ 20 nm thick). Serial overview
619 images of the entire embryo as well as high magnification and high-resolution
620 images of the cotyledon tips were collected with a Zeiss Merlin Compact SEM fitted
621 with a Gatan 3View system. Microscope settings were: 4 kV, 50 Pa at variable
622 pressure mode, 30 µm aperture. 3View settings were: 100 nm sections, pixel size ~
623 0.004 µm, pixel dwell time 3 µsec for high mag images and 2 µsec for overview
624 images.
625
626 **3D reconstruction**

627 The IMOD software package was used for stack formation, image alignment,
628 trimming and Gaussian filtering. Rendering of structures of interest was done in
629 Amira Software (FEI) using the magic wand tool to semi-automatically segment the
630 EV and PSV and the brush to manually segment the plasma membrane and
631 nucleus. Labels were modelled using surface generation and the number of triangles
632 reduced for visualisation. Movies were generated using the Animation tool in Amira.
633
634 **Acknowledgements**

635 This work was funded by the Leverhulme Trust (grant RPG-327 to LF) and the
636 BBSRC (grants BB/J017582/1 to LF and BB/M000168/1 to CH). We thank J.
637 Richardson and I. Hands-Portman for technical support. We are grateful to J. Harada
638 for donating *35S:LEC2-GR* seeds, J. Rogers and T. Okita for donating the anti-
639 TIP1;1 and anti-TIP3;1 antibodies, I. Hara-Nishimura for donating the anti-12S

antibody, A. Scarafoni for donating the anti-2S antibody, L. Jiang for the *35S:2S1-GFP* construct, A. Vitale for the gift of the *35S:TPK1-GFP* seeds and the anti-complex glycan antibody and K. Schumacher for donating *35S:VHA-a3-RFP* seeds.

FIGURE LEGENDS

Figure 1. Hypotheses for protein storage vacuole (PSV) formation tested in this work.

(A) PSV form *de novo*, briefly coexisting with the embryonic vacuole (EV) to eventually become the dominant structure in mature seeds. **(B)** PSV arise through reprogramming of the EV by accumulation of seed storage proteins in the EV lumen (green pattern fill). PSV-specific tonoplast markers (green outline) appear alongside the EV tonoplast markers (red outline) and coexist (yellow outline) while the EV is converted to a PSV.

Figure 2. Stages assigned to Arabidopsis embryo development and an overview of PSV formation in a representative cell from selected stages. **(A)** Images of heart, torpedo, walking stick and bent cotyledon embryos dissected from Arabidopsis ovules. The mature embryo was dissected from a dry seed. Bar = 100 µm. **(B)** PSV arise during the maturation phase of embryonic development. Panel shows single micrographs from SBF-SEM stacks of embryos at different developmental stages. Deposits of electron opaque material (arrow) are first observed in the vacuole lumen and along the tonoplast of the EV in early-bent cotyledon embryos. The deposits accumulate and eventually fill the vacuolar lumen in mature seed. Asterisks: oil bodies. Left scale bar for high magnification images = 1 µm. Right scale bar for overview images = 100 µm.

Figure 3. PSV tonoplast markers appear on the pre-existing EV tonoplast in bent cotyledon embryos. **(A-L)** Embryos constitutively expressing the tonoplast marker *35S:TPK-GFP* (green) and the PSV tonoplast markers (red) *TIP3;1:TIP3;1-YFP* (top and middle panels) or *TIP3;2:TIP3;2-mCherry* (bottom panel). Chlorophyll autofluorescence (blue). **(A-D)** In early-bent cotyledon embryos, the EV is labelled with TPK-GFP before PSV markers are expressed. **(E-L)** In later-stage bent cotyledon embryos, PSV tonoplast markers co-localise with the EV tonoplast marker. Bar = 5 µm.

Figure 4. 2S1 albumin seed storage proteins begin to accumulate in punctate cytosolic structures and ultimately as deposits inside lumina of forming PSV in bent cotyledon embryos. **(A-H)** 2S1-GFP (green) labels small punctate structures (arrows) and accumulates in the EV/PSV lumen (asteriks). The PSV tonoplast marker TIP3;2-mCherry (red) is localised to the ER, tonoplast and plasma membrane (empty arrowheads). Chlorophyll is shown in blue. **(A-D)** 2S1-GFP signal is first observed as small punctate structures in the cytoplasm and accumulates in PSV lumina whose tonoplasts are labelled with TIP3;2-mCherry. **(E-H)** In late-bent cotyledon embryos, the 2S1-GFP signal is observed only in vacuole lumina. Sub-regions of more intense 2S1-GFP fluorescence are visible in PSV lumina (arrowheads). Bar = 5 µm.

Figure 5. Forming PSV are identified by the acidotropic stains NR and BCECF-AM as well as PSV luminal autofluorescence in bent cotyledon embryos. **(A-H)** NR and BCECF-AM stain vacuoles labelled with the tonoplast markers TPK-GFP **(A)** or VHA-a3-RFP **(E**), respectively. Vacuole lumen autofluorescence (blue) co-localises with the stains **(D, H)**. **(I-L)** Embryos accumulating 2S1 albumin-GFP were stained with NR. The 2S1-GFP signal fills vacuole lumina and areas of more intense GFP fluorescence are observed (arrowheads) **(I)**. NR stains distinct sub-regions of vacuole lumina **(J)**. These NR-stained sub-regions co-localise with PSV lumen autofluorescence **(K)** and to areas of intense 2S1-GFP fluorescence **(L)**. Bar = 10 µm **(A-H)** and 5 µm **(I-L)**.

Figure 6. The PSV tonoplast aquaporin TIP3;1 as well as the 2S albumin and 12S globulin seed storage proteins are localised to the EV by immunogold labelling in bent cotyledon embryo cells. **(A-B)** Anti-TIP3;1 antibody labels the tonoplast of transitioning vacuoles. **(C-D)** Anti-12S globulin antibody labels electron opaque material accumulating along the luminal side of the tonoplast **(C)** and the entire PSV lumen in late-bent cotyledon embryos **(D)**. **(E-F)** Anti-2S antibody labels electron opaque material accumulating along the luminal side of the tonoplast **(E)** as well as electron opaque material in the vacuole lumen **(F)**. Oil bodies (OB). Bar = 500 nm.

Figure 7. PSV form by a remodelling of the LV in Arabidopsis leaf cells reprogrammed by LEC2. **(A-P)** Representative images of transitioning vacuoles in

LEC2-induced leaf cells at 14 **(A-D)**, 17 **(E-H)** and 20 **(I-P)** days on DEX. The TIP3;1-YFP PSV tonoplast marker (red) accumulates on the pre-existing LV **(E, I, M)** in Arabidopsis lines constitutively expressing the tonoplast marker TPK-GFP (green). Chlorophyll autofluorescence is shown in blue. Asterisk shows asynchronous remodelling of tonoplast in neighbouring cells. Bar = 10 μm. **(Q-T)** Electron microscopy of leaf cells 14 days after LEC2 induction with DEX. Electron opaque PSV material (black) accumulates along the luminal side of the tonoplast and disperses in the vacuole lumen. Bar = 500 nm **(Q-S)** and 2 μm **(T).**

Figure. 8. Tonoplast undergoes extensive remodelling during the LV-to-PSV transition in LEC2-induced leaf cells. **(A-F)** Representative images showing the progression of tonoplast remodelling during the LV-to-PSV transition at 14 **(A)**, 17 **(B, C)**, and 20 **(E)** days on DEX, or on 14 days without DEX **(F)**. Arabidopsis *35S:LEC2-GR* lines harbouring *35S:TPK1-GFP* (green) were imaged. Images are maximum intensity projections of Z-stacks taken through leaf epidermal cells. Bar = 10 μm.

Figure 9. Remodelling of the EV to PSV during embryo maturation. The lumen of the EV (blue), electron-opaque PSV luminal material (green), nucleus (yellow) and plasma membrane (grey) were rendered from SBF-SEM image stacks in cotyledon cells of embryos in the torpedo, early-, mid- and late-bent cotyledon or mature embryo stages. As electron-opaque material initially accumulates along the periphery of the EV lumen, the vacuole separates into several smaller vacuoles which are eventually filled with electron-opaque PSV luminal material aside from small remains. The nucleus changes position from the cell cortex to the centre of the cell. Bar = 5 μm.

Supplemental Figure S1. Punctate cytosolic 2S1-GFP-labelled structures associate with FM4-64-stained structures and appear to accumulate in vacuole lumina. **(A-B)** Bent cotyledon embryos expressing *2S1:2S1-GFP* (green) were long-term stained with FM4-64 (red). Chlorophyll autofluorescence is shown in blue. **(A)** High resolution Zeiss Airyscan detection shows punctate 2S1-GFP structures that appear to localise with brightly stained FM4-64 structures (arrowheads). **(B)** Punctate 2S1-

GFP structures also appear to accumulate within EV lumina (arrows). Bar = 5 µm **(C)** or 2 µm **(D)**.

Supplemental Figure S2. Fluorescently-labelled PSV tonoplast and lumen markers associate with the pre-existing EV. **(A-H)** The PSV (yellow) and EV (red) tonoplast markers label the tonoplast as well as ER and plasma membrane (filled arrowheads) in bent cotyledon embryo cells. The PSV lumen marker 2S1 albumin-GFP (green) labels small punctate structures (arrows) and accumulates in the EV/PSV lumina (asterisks). Silencing of the TIP1;1-RFP marker is observed in some cells of this line (empty arrowheads). **(A-D)** At the onset of PSV marker accumulation, the PSV tonoplast marker co-localises with the EV marker. **(E-H)** 2S1-GFP accumulates in the vacuole labelled by both EV and PSV markers. Sub-regions of more intense 2S1-GFP fluorescence are visible in vacuole lumina (empty arrows). Bar = 5 µm.

Supplemental Figure S3. NR staining pattern and appearance of PSV autofluorescence in EV/PSV of bent cotyledon embryos. **(A-F)** Bent cotyledon embryos expressing *TIP3;1:YFP-TIP3;1* or *TIP3;1:TIP3;1-YFP* (green) were stained with NR (red) **(A-C)** or imaged for PSV autofluorescence (blue) **(D-F)**. Embryos were isolated from green siliques **(A, B, D-F)** or from yellowing siliques **(C)**. Inset shows embryos imaged. **(A, D)** NR **(A)** and PSV autofluorescence **(D)** appear in distinct sub-regions of EV/PSV lumina. **(B, E)** NR **(B)** and PSV autofluorescence **(E)** signals occupy a greater volume of EV/PSV lumina. **(C, F)** The entire PSV lumen is stained with NR **(C)** or autofluoresces **(F)**. Bar = 5 µm **(A, C-E)** and 10 µm **(B, F)**.

Supplemental Figure S4. Immunogold labelling of the 2S albumin seed storage proteins in torpedo **(A)** and early- **(B, C)** to mid-walking stick **(D)** embryos show no significant signal. Only very few gold particles can be detected (red circle). Bar = 500 nm.

Supplemental Figure S5. Highlighted gold particles (red circles) indicating immunogold labelling with antibodies against TIP3;1 **(A', B')**, 12S globulins **(C', D')** and 2S albumins **(E', F')** in the cells shown in Figure 6. Bar = 500 nm.

Supplemental Figure S6. Anti-complex glycan antibody labelling in early- and late-bent cotyledon embryos. **(A)** Gold is first detected along the tonoplast of the EV**.** Oil bodies (OB). **(B)** In cells of late-bent cotyledon embryos the entire PSV is labelled. **(A', B')** Highlighted gold particles (red circles) indicating immunogold labelling with antibodies against complex glycan shown in A and B. Bar = 500 nm.

Supplemental Fig. S7. Vacuoles exhibit highly dynamic remodelling during the LV-to-PSV transition in LEC2-induced leaf epidermal cells. **(A-F)** Representative cells of an Arabidopsis 35S:LEC2-GR line expressing 35S:TPK1-GFP (green) after 18 days on DEX **(A-C)** or after 14 days without DEX **(D-F)**. Images show tonoplast remodelling at frame 1 **(A, D)** and frame 120 **(B, E)** of the time series. Time series images were acquired over 150 sec and data are also displayed as temporal colour-coded images using FIJI **(C, F)**. Spectrum LUT colour scale bar shows tonoplast movement, where white indicates no movement. Bar = 10 µm.

Supplemental Figure S8. Regions of interest (ROI) of selected embryos at different developmental stages imaged with SBF-SEM. ROIs used for reconstructions of torpedo (Suppl. Movie 3), early-bent cotyledon (Suppl. Movie 5), late-bent cotyledon (Suppl. Movie 7) and mature seed (Suppl. Movie 9) are highlighted in yellow boxes.

Supplemental Figure S9. Cross section view through vacuoles in cotyledon cells of embryos in the torpedo, early-, mid- and late-bent cotyledon and mature embryo stages. **(A)** Original SBF-SEM image. **(B)** Semi-transparent SBF-SEM images with underlying 3D reconstruction of the EV (blue) and PSV (green). **(C)** Cross sectioned vacuole reconstruction alone. **(D)** Tilted view of the reconstruction. Bar = 5 µm.

Supplemental Figure S10. Storage proteins accumulate within the lumen of the pre-existing vacuole. (**A-B)** the electron-opaque storage protein aggregate in the EV from early bent cotyledons is not surrounded by a membrane. The inset in A indicates the area magnified in B. Asterisks show a clearly define interface between the embryonic vacuole (EV) and the oil body (OB).
(C-D) Anti-TIP3;1 antibody labels the tonoplast of transitioning vacuoles in LEC2-induced leaf cells. The inset in C indicates the area magnified in D. Note that the

gold labelling is only found on the outer edge of the storage protein aggregates (arrows). Scale bars: 500nm

Supplemental Movie 1. Arabidopsis *35S:LEC2-GR* line expressing *35S:TPK1-GFP* (green) after 18 days on DEX. A cell in the leaf epidermis was imaged to show tonoplast remodelling as a 2D time series.

Supplemental Movie 2. Arabidopsis *35S:LEC2-GR* line expressing *35S:TPK1-GFP* (green) after 14 days without DEX. A cell in the leaf epidermis was imaged to show tonoplast remodelling as a 2D time series.

Supplemental Movie 3. 3D Reconstruction of one cell in the cotyledon of a torpedo staged embryo. Volume rendering of the entire image stack is shown rotating, then an orthoslice moving through the image stack from start to end and back. The modelled lumen of EV appears in blue, the PSV material appears in green, the nucleus appears in yellow and finally the cell membrane appears in transparent grey.

Supplemental Movie 4. Orthoslice moving through the image stack from a torpedo staged embryo cotyledon from which the cell was extracted from 3D reconstruction.

Supplemental Movie 5. 3D Reconstruction of one cell in the cotyledon of an early bent cotyledon staged embryo. Volume rendering of the entire image stack is shown rotating, then an orthoslice moving through the image stack from start to end and back. The modelled lumen of EV appears in blue, the PSV material appears in green, the nucleus appears in yellow and finally the cell membrane appears in transparent grey.

Supplemental Movie 6. Orthoslice moving through the image stack from an early bent cotyledon staged embryo cotyledon from which the cell was extracted from 3D reconstruction.

Supplemental Movie 7. 3D Reconstruction of one cell in the cotyledon of a late bent cotyledon staged embryo. Volume rendering of the entire image stack is shown rotating, then an orthoslice moving through the image stack from start to end and

back. The modelled lumen of EV appears in blue, the PSV material appears in green, the nucleus appears in yellow and finally the cell membrane appears in transparent grey.

Supplemental Movie 8. Orthoslice moving through the image stack from a late bent cotyledon staged embryo cotyledon from which the cell was extracted from 3D reconstruction.

Supplemental Movie 9. 3D Reconstruction of one cell in the cotyledon of a mature seed staged embryo. Volume rendering of the entire image stack is shown rotating, then an orthoslice moving through the image stack from start to end and back. The modelled lumen of EV appears in blue, the PSV material appears in green, the nucleus appears in yellow and finally the cell membrane appears in transparent grey.

Supplemental Movie 10. Orthoslice moving through the image stack from a mature staged embryo cotyledon from which the cell was extracted from 3D reconstruction.

Parsed Citations

Bagga S, Sutton D, Kemp JD, Sengupta-Gopalan C (1992) Constitutive expression of the □-phaseolin gene in different tissues of transgenic alfalfa does not ensure phaseolin accumulation in non-seed tissue. Plant Mol Biol 19: 951-958

Pubmed: Author and Title
CrossRef: Author and Title
Google Scholar: Author Only Title Only Author and Title

Baud S, Kelemen Z, Thévenin J, Boulard C, Blanchet S, To A, Payre M, Berger N, Effroy-Cuzzi D, Franco-Zorrilla JM, Godoy M, Solano R, Thevenon E, Parcy F, Lepiniec L, Dubreucq B (2016) Deciphering the molecular mechanisms underpinning the transcriptional control of gene expression by master transcriptional regulators in Arabidopsis seed. Plant Physiol 171: 1099-1112

Pubmed: Author and Title
CrossRef: Author and Title
Google Scholar: Author Only Title Only Author and Title

Bolte S, Lanquar V, Soler M-N, Beebo A, Satiat-Jeunemaître B, Bouhidel K, Thomine S (2011) Distinct lytic vacuolar compartments are embedded inside the protein storage vacuole of dry and germinating Arabidopsis thaliana seeds. Plant Cell Physiol 52: 1142-1152

Pubmed: Author and Title
CrossRef: Author and Title
Google Scholar: Author Only Title Only Author and Title

Bolte S, Talbot C, Boutte Y, Catrice O, Read ND, Satiat-Jeunemaitre B (2004) FM-dyes as experimental probes for dissecting vesicle trafficking in living plant cells. J Microsc 214: 159-173

Pubmed: Author and Title
CrossRef: Author and Title
Google Scholar: Author Only Title Only Author and Title

Braybrook SA, Harada JJ (2008) LECs go crazy in embryo development. Trends Plant Sci 13: 624-630

Pubmed: Author and Title
CrossRef: Author and Title
Google Scholar: Author Only Title Only Author and Title

Brux A, Liu TY, Krebs M, Stierhof YD, Lohmann JU, Miersch O, Wasternack C, Schumacher K (2008) Reduced V-ATPase activity in the trans-Golgi network causes oxylipin-dependent hypocotyl growth inhibition in Arabidopsis. Plant Cell 20: 1088-1100

Pubmed: Author and Title
CrossRef: Author and Title
Google Scholar: Author Only Title Only Author and Title

D'Ippólito S, Arias LA, Casalongué CA, Pagnussat GC, Fiol DF (2017) The DC1-domain protein VACUOLELESS GAMETOPHYTES is essential for female and male gametophyte development in Arabidopsis. Plant J 90: 261-275

Pubmed: Author and Title
CrossRef: Author and Title
Google Scholar: Author Only Title Only Author and Title

De D (2000) Plant cell vacuoles. CSIRO Publishing, Collingwood, Australia

Pubmed: Author and Title
CrossRef: Author and Title
Google Scholar: Author Only Title Only Author and Title

Dettmer J, Hong-Hermesdorf A, Stierhof Y-D, Schumacher K (2006) Vacuolar H-ATPase activity is required for endocytic and secretory trafficking in Arabidopsis. Plant Cell 18: 715-730

Pubmed: Author and Title
CrossRef: Author and Title
Google Scholar: Author Only Title Only Author and Title

Dubrovsky JG, Guttenberger M, Saralegui A, Napsucialy-Mendivil S, Voigt B, Baluska F, Menzel D (2006) Neutral red as a probe for confocal laser scanning microscopy studies of plant roots. Ann Bot 97: 1127-1138

Pubmed: Author and Title
CrossRef: Author and Title
Google Scholar: Author Only Title Only Author and Title

Ebine K, Okatani Y, Uemura T, Goh T, Shoda K, Niihama M, Morita MT, Spitzer C, Otegui MS, Nakano A, Ueda T (2008) A SNARE complex unique to seed plants is required for protein storage vacuole biogenesis and seed development of Arabidopsis thaliana. Plant Cell 20: 3006-3021

Pubmed: Author and Title
CrossRef: Author and Title
Google Scholar: Author Only Title Only Author and Title

Feeney M, Frigerio L, Cui Y, Menassa R (2013a) Following vegetative to embryonic cellular changes in leaves of Arabidopsis by overexpressing LEAFY COTYLEDON2. Plant Physiol 162: 1881-1896

Pubmed: Author and Title
CrossRef: Author and Title
Google Scholar: Author Only Title Only Author and Title

Feeney M, Frigerio L, Kohalmi SE, Cui Y, Menassa R (2013b) Reprogramming cells to study vacuolar development. Front Plant Sci 4: 493
Pubmed: Author and Title
CrossRef: Author and Title
Google Scholar: Author Only Title Only Author and Title

Frigerio L, de Virgilio M, Prada A, Faoro F, Vitale A (1998) Sorting of phaseolin to the vacuole is saturable and requires a short C-terminal peptide. Plant Cell 10: 1031-1042
Pubmed: Author and Title
CrossRef: Author and Title
Google Scholar: Author Only Title Only Author and Title

Frigerio L, Hinz G, Robinson DG (2008) Multiple vacuoles in plant cells: rule or exception? Traffic 9: 1564-1570
Pubmed: Author and Title
CrossRef: Author and Title
Google Scholar: Author Only Title Only Author and Title

Frigerio L, Vine ND, Pedrazzini E, Hein MB, Wang F, Ma JK-C, Vitale A (2000) Assembly, secretion and vacuolar delivery of a hybrid immunoglobulin in plants. Plant Physiol 123: 1483 -1493
Pubmed: Author and Title
CrossRef: Author and Title
Google Scholar: Author Only Title Only Author and Title

Fuji K, Shimada T, Takahashi H, Tamura K, Koumoto Y, Utsumi S, Nishizawa K, Maruyama N, Hara-Nishimura I (2007) Arabidopsis vacuolar sorting mutants (green fluorescent seed) can be identified efficiently by secretion of vacuole-targeted green fluorescent protein in their seeds. Plant Cell 19: 597-609
Pubmed: Author and Title
CrossRef: Author and Title
Google Scholar: Author Only Title Only Author and Title

Gao C, Zhuang X, Cui Y, Fu X, He Y, Zhao Q, Zeng Y, Shen J, Luo M, Jiang L (2015) Dual roles of an Arabidopsis ESCRT component FREE1 in regulating vacuolar protein transport and autophagic degradation. Proc Natl Acad Sci USA 112: 1886-1891
Pubmed: Author and Title
CrossRef: Author and Title
Google Scholar: Author Only Title Only Author and Title

Gattolin S, Sorieul M, Frigerio L (2011) Mapping of tonoplast intrinsic proteins in maturing and germinating Arabidopsis seeds reveals dual localization of embryonic TIPs to the tonoplast and plasma membrane. Mol Plant 4: 180-189
Pubmed: Author and Title
CrossRef: Author and Title
Google Scholar: Author Only Title Only Author and Title

Gattolin S, Sorieul M, Hunter PR, Khonsari R, Frigerio L (2009) Expression mapping of the tonoplast intrinsic protein family in Arabidopsis root tissues. BMC Plant Biol 9: 133
Pubmed: Author and Title
CrossRef: Author and Title
Google Scholar: Author Only Title Only Author and Title

Gillespie J, Rogers SW, Deery M, Dupree P, Rogers JC (2005) A unique family of proteins associated with internalized membranes in protein storage vacuoles of the Brassicaceae. Plant J 41: 429-441
Pubmed: Author and Title
CrossRef: Author and Title
Google Scholar: Author Only Title Only Author and Title

Hara-Nishimura I, Hayashi M, Nishimura M, Akazawa T (1987) Biogenesis of protein bodies by budding from vacuoles in developing pumpkin cotyledons. Protoplasma 136: 49-55
Pubmed: Author and Title
CrossRef: Author and Title
Google Scholar: Author Only Title Only Author and Title

Harris LJ, Gleddie SC (2001) A modified Rpl3 gene from rice confers tolerance of the Fusarium graminearum mycotoxin deoxynivalenol to transgenic tobacco. Physiol Mol Plant Pathol 58: 173-181
Pubmed: Author and Title
CrossRef: Author and Title
Google Scholar: Author Only Title Only Author and Title

Hegedus DD, Coutu C, Harrington M, Hope B, Gerbrandt K, Nikolov I (2015) Multiple internal sorting determinants can contribute to the trafficking of cruciferin to protein storage vacuoles. Plant Mol Biol 88: 3-20
Pubmed: Author and Title
CrossRef: Author and Title
Google Scholar: Author Only Title Only Author and Title

Hoh B, Hinz G, Jeong BK, Robinson DG (1995) Protein storage vacuoles form de novo during pea cotyledon development. J Cell Sci 108: 299-310
Pubmed: Author and Title

CrossRef: Author and Title
Google Scholar: Author Only Title Only Author and Title

Hunter PR, Craddock CP, Di Benedetto S, Roberts LM, Frigerio L (2007) Fluorescent reporter proteins for the tonoplast and the vacuolar lumen identify a single vacuolar compartment in Arabidopsis cells. Plant Physiol 145: 1371-1382
Pubmed: Author and Title
CrossRef: Author and Title
Google Scholar: Author Only Title Only Author and Title

Jauh G-Y, Phillips TE, Rogers JC (1999) Tonoplast intrinsic protein isoforms as markers for vacuolar functions. Plant Cell 11: 1867-1882
Pubmed: Author and Title
CrossRef: Author and Title
Google Scholar: Author Only Title Only Author and Title

Jiang L, Phillips TE, Hamm CA, Drozdowicz YM, Rea PA, Maeshima M, Rogers SW, Rogers JC (2001) The protein storage vacuole: a unique compound organelle. J Cell Biol 155: 991-1002
Pubmed: Author and Title
CrossRef: Author and Title
Google Scholar: Author Only Title Only Author and Title

Jiang L, Phillips TE, Rogers SW, Rogers JC (2000) Biogenesis of the protein storage vacuole crystalloid. J Cell Biol 150: 755-769
Pubmed: Author and Title
CrossRef: Author and Title
Google Scholar: Author Only Title Only Author and Title

Johnson KD, Höfte H, Chrispeels MJ (1990) An intrinsic tonoplast protein of protein storage vacuoles in seeds is structurally related to a bacterial solute transporter (GlpF). Plant Cell 2: 525-532
Pubmed: Author and Title
CrossRef: Author and Title
Google Scholar: Author Only Title Only Author and Title

Kittelmann M, Hawes C, Hughes L (2016) Serial block face scanning electron microscopy and the reconstruction of plant cell membrane systems. J Microsc 263: 200-211
Pubmed: Author and Title
CrossRef: Author and Title
Google Scholar: Author Only Title Only Author and Title

Kolb C, Nagel M-K, Kalinowska K, Hagmann J, Ichikawa M, Anzenberger F, Alkofer A, Sato MH, Braun P, Isono E (2015) FYVE1 Is essential for vacuole biogenesis and intracellular trafficking in Arabidopsis. Plant Physiol 167: 1361-1373
Pubmed: Author and Title
CrossRef: Author and Title
Google Scholar: Author Only Title Only Author and Title

Lauriere M, Lauriere C, Chrispeels MJ, Johnson KD, Sturm A (1989) Characterization of a xylose-specific antiserum that reacts with the complex asparagine-linked glycans of extracellular and vacuolar glycoproteins. Plant Physiol 90: 1182-1188
Pubmed: Author and Title
CrossRef: Author and Title
Google Scholar: Author Only Title Only Author and Title

Maitrejean M, Wudick MM, Voelker C, Prinsi B, Mueller-Roeber B, Czempinski K, Pedrazzini E, Vitale A (2011) Assembly and sorting of the tonoplast potassium channel AtTPK1 and its turnover by internalization into the vacuole. Plant Physiol 156: 1783-1796
Pubmed: Author and Title
CrossRef: Author and Title
Google Scholar: Author Only Title Only Author and Title

Mansfield SG, Briarty LG (1992) Cotyledon cell development in Arabidopsis thaliana during reserve deposition. Can J Bot 70: 151-164
Pubmed: Author and Title
CrossRef: Author and Title
Google Scholar: Author Only Title Only Author and Title

Marty F (1999) Plant vacuoles. Plant Cell 11: 587-600
Pubmed: Author and Title
CrossRef: Author and Title
Google Scholar: Author Only Title Only Author and Title

Miao Y, Li KY, Li HY, Yao X, Jiang L (2008) The vacuolar transport of aleurain-GFP and 2S albumin-GFP fusions is mediated by the same pre-vacuolar compartments in tobacco BY-2 and Arabidopsis suspension cultured cells. Plant J 56: 824-839
Pubmed: Author and Title
CrossRef: Author and Title
Google Scholar: Author Only Title Only Author and Title

Olbrich A, Hillmer S, Hinz G, Oliviusson P, Robinson DG (2007) Newly formed vacuoles in root meristems of barley and pea seedlings have characteristics of both protein storage and lytic vacuoles. Plant Physiol 145: 1383-1394
Pubmed: Author and Title
CrossRef: Author and Title
Google Scholar: Author Only Title Only Author and Title

Otegui MS, Capp R, Staehelin LA (2002) Developing seeds of Arabidopsis store different minerals in two types of vacuoles and in the endoplasmic reticulum. Plant Cell 14: 1311-1327
Pubmed: Author and Title
CrossRef: Author and Title
Google Scholar: Author Only Title Only Author and Title

Otegui MS, Herder R, Schulze J, Jung R, Staehelin LA (2006) The proteolytic processing of seed storage proteins in Arabidopsis embryo cells starts in the multivesicular bodies. Plant Cell 18: 2567-2581
Pubmed: Author and Title
CrossRef: Author and Title
Google Scholar: Author Only Title Only Author and Title

Reynolds ES (1963) The use of lead citrate at high pH as an electron-opaque stain in electron microscopy. J Cell Biol 17: 208-212
Pubmed: Author and Title
CrossRef: Author and Title
Google Scholar: Author Only Title Only Author and Title

Rojo E, Gillmor CS, Kovaleva V, Somerville CR, Raikhel NV (2001) VACUOLELESS1 is an essential gene required for vacuole formation and morphogenesis in Arabidopsis. Dev Cell 1: 303-310
Pubmed: Author and Title
CrossRef: Author and Title
Google Scholar: Author Only Title Only Author and Title

Sanmartin M, Ordonez A, Sohn EJ, Robert S, Sanchez-Serrano JJ, Surpin MA, Raikhel NV, Rojo E (2007) Divergent functions of VTI12 and VTI11 in trafficking to storage and lytic vacuoles in Arabidopsis. Proc Natl Acad Sci USA 104: 3645-3650
Pubmed: Author and Title
CrossRef: Author and Title
Google Scholar: Author Only Title Only Author and Title

Scarafoni A, Carzaniga R, Harris N, Croy RR (2001) Manipulation of the napin primary structure alters its packaging and deposition in transgenic tobacco (Nicotiana tabacum L.) seeds. Plant Mol Biol 46: 727-739
Pubmed: Author and Title
CrossRef: Author and Title
Google Scholar: Author Only Title Only Author and Title

Scheuring D, Schöller M, Kleine-Vehn J, Löfke C (2015) Vacuolar staining methods in plant cells. In JM Estevez, ed, Plant Cell Expansion: Methods and Protocols. Springer New York, New York, NY, pp 83-92
Pubmed: Author and Title
CrossRef: Author and Title
Google Scholar: Author Only Title Only Author and Title

Scheuring D, Viotti C, Krüger F, Künzl F, Sturm S, Bubeck J, Hillmer S, Frigerio L, Robinson DG, Pimpl P, Schumacher K (2011) Multivesicular bodies mature from the trans-Golgi network/early endosome in Arabidopsis. Plant Cell 23: 3463-3481
Pubmed: Author and Title
CrossRef: Author and Title
Google Scholar: Author Only Title Only Author and Title

Shimada T, Yamada K, Kataoka M, Nakaune S, Koumoto Y, Kuroyanagi M, Tabata S, Kato T, Shinozaki K, Seki M, Kobayashi M, Kondo M, Nishimura M, Hara-Nishimura I (2003) Vacuolar processing enzymes are essential for proper processing of seed storage proteins in Arabidopsis thaliana. J Biol Chem 278: 32292-32299
Pubmed: Author and Title
CrossRef: Author and Title
Google Scholar: Author Only Title Only Author and Title

Sohn EJ, Rojas-Pierce M, Pan S, Carter C, Serrano-Mislata A, Madueno F, Rojo E, Surpin M, Raikhel NV (2007) The shoot meristem identity gene TFL1 is involved in flower development and trafficking to the protein storage vacuole. Proc Natl Acad Sci USA 104: 18801-18806
Pubmed: Author and Title
CrossRef: Author and Title
Google Scholar: Author Only Title Only Author and Title

Stone SL, Braybrook SA, Paula SL, Kwong LW, Meuser J, Pelletier J, Hsieh T-F, Fischer RL, Goldberg RB, Harada JJ (2008) Arabidopsis LEAFY COTYLEDON2 induces maturation traits and auxin activity: Implications for somatic embryogenesis. Proc Natl Acad Sci USA 105: 3151-3156
Pubmed: Author and Title
CrossRef: Author and Title
Google Scholar: Author Only Title Only Author and Title

Stone SL, Kwong LW, Yee KM, Pelletier J, Lepiniec L, Fischer RL, Goldberg RB, Harada JJ (2001) LEAFY COTYLEDON2 encodes a B3 domain transcription factor that induces embryo development. Proc Natl Acad Sci USA 98: 11806-11811
Pubmed: Author and Title
CrossRef: Author and Title
Google Scholar: Author Only Title Only Author and Title

Tse YC, Mo B, Hillmer S, Zhao M, Lo SW, Robinson DG, Jiang L (2004) Identification of multivesicular bodies as prevacuolar

compartments in Nicotiana tabacum BY-2 cells. Plant Cell 16: 672-693
Pubmed: Author and Title
CrossRef: Author and Title
Google Scholar: Author Only Title Only Author and Title

Vicente-Carbajosa J, Carbonero P (2005) Seed maturation: developing an intrusive phase to accomplish a quiescent state. Int J Dev Biol 49: 645-651
Pubmed: Author and Title
CrossRef: Author and Title
Google Scholar: Author Only Title Only Author and Title

Viotti C, Bubeck J, Stierhof Y-D, Krebs M, Langhans M, van den Berg W, van Dongen W, Richter S, Geldner N, Takano J, Jürgens G, de Vries SC, Robinson DG, Schumacher K (2010) Endocytic and secretory traffic in Arabidopsis merge in the trans-Golgi network/early endosome, an independent and highly dynamic organelle. Plant Cell 22: 1344-1357
Pubmed: Author and Title
CrossRef: Author and Title
Google Scholar: Author Only Title Only Author and Title

Voelker C, Schmidt D, Mueller-Roeber B, Czempinski K (2006) Members of the Arabidopsis AtTPK/KCO family form homomeric vacuolar channels in planta. Plant J 48: 296-306
Pubmed: Author and Title
CrossRef: Author and Title
Google Scholar: Author Only Title Only Author and Title

West MAL, Harada JJ (1993) Embryogenesis in higher plants: an overview. Plant Cell 5: 1361-1369
Pubmed: Author and Title
CrossRef: Author and Title
Google Scholar: Author Only Title Only Author and Title

Zheng H, Staehelin LA (2011) Protein storage vacuoles are transformed into lytic vacuoles in root meristematic cells of germinating seedlings by multiple, cell type-specific mechanisms. Plant Physiol 155: 2023-2035
Pubmed: Author and Title
CrossRef: Author and Title
Google Scholar: Author Only Title Only Author and Title

Zheng J, Han SW, Rodriguez-Welsh MF, Rojas-Pierce M (2014) Homotypic vacuole fusion requires VTI11 and is regulated by phosphoinositides. Mol Plant 7: 1026-1040
Pubmed: Author and Title
CrossRef: Author and Title
Google Scholar: Author Only Title Only Author and Title

Zwiewka M, Feraru E, Moller B, Hwang I, Feraru MI, Kleine-Vehn J, Weijers D, Friml J (2011) The AP-3 adaptor complex is required for vacuolar function in Arabidopsis. Cell Res 21: 1711-1722
Pubmed: Author and Title
CrossRef: Author and Title
Google Scholar: Author Only Title Only Author and Title